Republic of Iraq
Ministry of Higher Education
and Scientific Research
University of Babylon
College of Education for Pure Sciences
Department of Physics

Effect of Si_3N_4-TaC Nanoparticles on PMMA Properties as Antibacterial

A Thesis

Submitted to the Council of the College of Education for Pure Sciences, University of Babylon in Partial Fulfillment of the Requirements for the Degree of Master in Education/ Physics

By

Alaa Abass Mohammed Telfah

B. Education Physics

University of Babylon (2009)

Supervised By

Prof. Dr. Majeed Ali Habeeb

2023 A.D. **1444 A.H**

بسم الله الرحمن الرحيم

" قالُوا سُبحانَك لا عِلمَ لَنا

إلا ما عَلمتَنا إنَكَ أنتَ العَليمُ الحكيمُ "

صدق الله العظيم

(سورة البقرة : آيه 32)

Supervisor's Certification

I certify that this thesis entitled (**Effect of Si_3N_4-TaC Nanoparticles on PMMA Properties as Antibacterial**) is prepared by th**e** student **Alaa Abass Mohammed Telfah** under my supervision at the College of Education for Pure Sciences, University of Babylon as partial fulfillment of the requirements for the Degree of Master in Education / Physics.

Signature:
Name: Dr. Majeed Ali Habeeb
Title: Professor
(Supervisor)
Date: / /2023

Head of the Department Certificate

In view of the available recommendations, I forward this thesis for debate by the Examining Committee.
Signature:
Name: Dr. Khalid Haneen Abass
Title: Professor
Head of phy Department
Date: / / 2023

Dedication

To whom God has shown with prestige and glory,
To the person who taught me tenderness without waiting,
To whom I carry my name with all pride,
my beloved father

I ask God to extend his age to see the fruit that has come to be harvested after a long period of waiting and his words will remain stars to guide me today, tomorrow and forever, To my angel in life,

To the meaning of love and the fountain of tenderness,

who was the prayer of the secret of my success,

my beloved mother

To my dear husband

I dedicate this study as an expression of my sincere thanks.

For what he gave me throughout my studies moral and material support, he was a good husband and friend

Alaa Abass

ACKNOWLEDGEMENTS

My first and foremost thanks are due to Allah Glorified and Exalted Be He without His continuous and everlasting assistance, blessings, and success the completion of this study would not be possible. My profoundest gratitude is to my supervisor **Prof. Dr. Majeed Ali Habeeb** for his extremely intellectual and stimulating generosity, discussions, encouragements, comments, and the time he spent in reviewing the thesis that helped to enrich and broaden my research thematically and systematically. His tremendous guidance, patience, and inspiring comments significantly have led to the fulfillment of the work. I would like to extend my sincere gratitude to **Prof. Dr. khalid Haneen** the head of the department of physics, college of education for pure sciences for his kind help.

Alaa Abass

Abstract

In this study, the Poly Methyl Methacrylate/Silicon Nitride/Tantalum Carbide (PMMA/Si_3N_4/TaC) nanocomposites has been prepared by using casting method with variant content of (Si_3N_4/TaC) nanoparticles (2, 4, 6 and 8) wt.%. The structural, morphological, optical and AC electrical properties of (PMMA/Si_3N_4/TaC) nanocomposites have been investigated.

The optical microscope images show that Si_3N_4 /TaC nanoparticles form a continuous network inside the polymers when the ratio of (8) wt.%. FTIR spectra show a shift in some bands and change in the intensities of other bands comparing with pure (PMMA) polymer, this indicates there is no interaction between the polymers and the added nanoparticles. FE-SEM images shows the surface morphology of the (PMMA/Si_3N_4/TaC) nanocomposites distributed homogeneous and regular inside polymer matrix.

The optical properties exhibited that the absorbance, absorption coefficient, refractive index, extinction coefficient, dielectric constant (real, imaginary) and optical conductivity of (PMMA/Si_3N_4/TaC) nanocomposites increased with the increasing of the concentrations of the (Si_3N_4/TaC) nanoparticles. The transmittance and the energy gap for indirect transition (allowed, forbidden) decreased with the increasing of the concentrations of (Si_3N_4/TaC) nanoparticles.

The AC electrical properties exhibited that the dielectric constant and dielectric loss for (PMMA/Si_3N_4/TaC) nanocomposites are increased with the increasing of (Si_3N_4/TaC) nanoparticles concentration and decreasing with the increase of frequency of the applied electric field. The A.C electrical conductivity increased with the increasing of (Si_3N_4/TaC)

nanoparticles concentration and frequency of the applied electric field frequency.

The (PMMA/Si_3N_4/TaC) nanocomposites were examined as antibacterial against gram-positive (Staphylococcus aureus) and gram-negative (Klebsiella aerogenes) and exhibited that the inhibition zone diameter increases with the increase in (Si_3N_4/TaC) nanoparticles concentrations.

List of contents

List of Tables

List of Figures

List of Symbols and Abbreviations

Symbols	Physical Meanings
$\sigma_{A.C}$	A.C electrical conductivity
I_A	Absorbed intensity of light
A	Absorbance
h	Plank constant
α	Absorption coefficient
Eact	Activation energy
w	Angular frequency
C	Capacitance
I_q	Capacitance current
ε	Complex dielectric constant
N	Complex refractive index
I_p	Conduction current
ε'	Dielectric constant
ε''	Dielectric loss
Tan δ	Dielectric loss tangent
k_o	Extinction coefficient
ε_i	Imaginary dielectric constant
Z	Impedance
I_o	Incident intensity of light
I_T	Intensity of transmittance
V_m	Maximum voltage
E_g^{opt}	Optical energy gap

R_P	**Parallel resistance**
E_{ph}	**Phonon energy**
C_p	**Parallel capacitance**
V	**Potential exerted**
ε_r	**Real dielectric constant**
n	**Refractive index**
t	**Thickness of the matter**
T	**Transmittance**
UV	**Ultraviolet spectrum**
C_o	**Vacuum capacitor**
ε_o	**Vacuum permittivity**
V.B	**Valens band**
c	**Velocity of light**
K	**Wave vector**
B	**Width polar**
PMMA	**Poly(methyl methacrylate)polymer**
Si_3N_4	**Silicon Nitrite**
TaC	**Tantalum Carbide**
FTIR	**Fourier Transformation Infrared Ray**
OM	**Optical Microscope**
FE-SEM	**Field Emission Scanning Electron Microscope**
C.B	**Conduction Band**
V.B	**Valence Band**
A.C	**Alternating current**

Chapter One

Introduction and Literature Review

1.1 Introduction

Polymers are materials consist of many small molecules, these macromolecules may be linear, branched, or highly network [1]. The small molecules used as the building blocks for these larger molecules are known as monomers. Monomers are small molecules can be joined together in a repetitive manner to form more complex molecules called polymers [2]. The process by which monomers are transformed into a polymer is called polymerization [3].

The polymerization process is the process that allows a simple low molecular weight compound to combine and form a high molecular weight complex .The Polymerization process can be classified into two types: condensation polymerization and addition polymerization [4,5]. Polymers can be divided into two categories according to their sources: natural and synthetic, natural polymers include proteins, cellulose, and rubber, while synthetic polymers include nylon, polypropylene, polyester, polycarbonate, and etc. [6].

The nanoparticle includes particles having size between 1 and 100 nm, these particles have different properties at their atomic level due to their size [7]. Can applied these particles in different fields such as pharmaceutical, nanoelectronics, and cosmetic [8]. The field of nanotechnology is one of the most popular areas of current research and development for basically all technical disciplines, and this obviously includes polymer science and technology [9]. Evan before nanotechnology was recognized as a new scientific field, work on the manufacture and production of nanomaterials and nanostructures began a long time ago [10].

Due to rapid technological advancements, some components currently used in manufacturing have to be replaced with new materials with improved specifications; as a result, studies of electrical and optical properties of polymers have gotten a lot of attention in recent years due to their usage in electronic and optical devices [11,12].

1.2 Polymer Structure

Polymers are large organic molecules (macromolecules) composed of small structural components (monomers) linked together in a polymerization process [13]. Each molecule is made up of thousands of atoms that are connected by covalent chemical bonds, and molecules in polymers are attracted to one another by forces that vary depending on the polymer type. Polymers with low temperatures have limited crystal connections because polymers are made up of big, linked molecules that are difficult to handle. A linear chain of molecules can only arrange itself in an orderly fashion in a few locations. In the solid state, polymers have crystalline and non-crystalline regions [14].

1.3 Classification of Polymers

1.3.1 Chemical Classification of Polymers

There are different kinds of polymers categorized according to their structure and as follows [15,16]:

1.3.1.1 Linear Polymers

Single molecular is the basic structural unit for polymers in a series of certain lengths that are connected in a linear form. Linear polymers may include totals twisted that are a part of monomer but without any branch, as revealed in figure (1-1a).

1.3.1.2 Branched Polymers

This type of polymers consists of several branches that could be a Ladder and Crusader or Comb, which is usually present with various lengths, as illustrated in figure (1-1 b).

1.3.1.3 Cross Linked Polymers

This kind of polymers consists of chains from three dimensional linked together in more than one site and monomers bonding in effective totals that are chemical bonds, as displayed in figure (1-1 c).

1.3.1.4 Network polymers

Three-dimensional (3D) networks are made of trifunctional. Examples: phenol-formaldehyde and epoxies, as in the figure (1-1d).

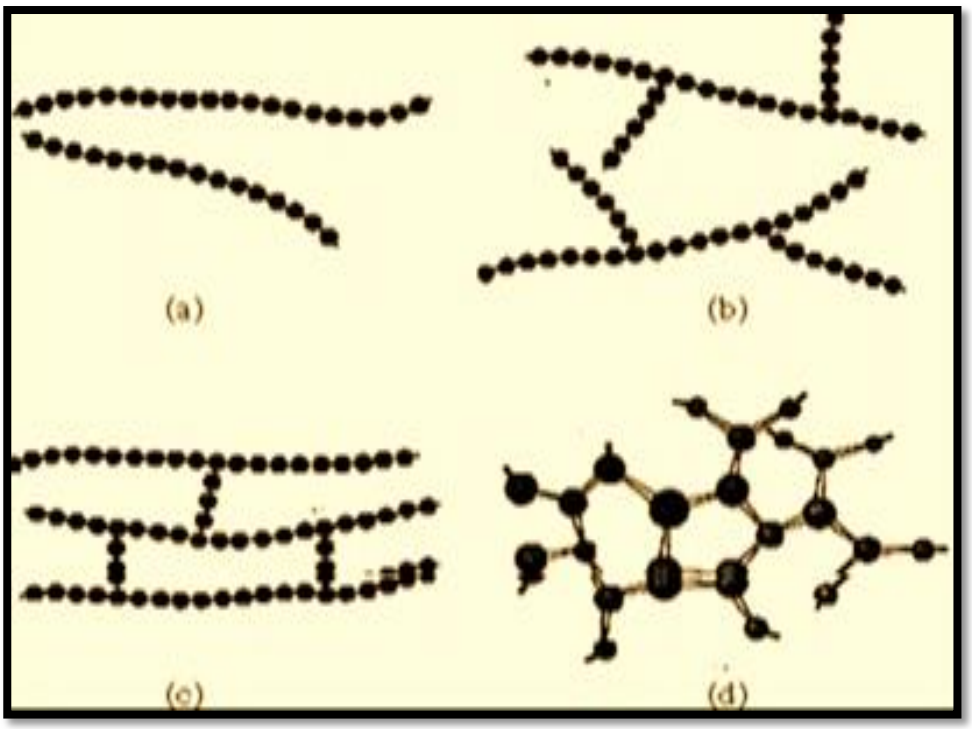

Fig. (1-1) Polymeric Chains Types (a) Linear, (b) Branched, (c) Cross-linked and (d) Network polymers [16] .

1.3.2 Classification of Polymers Dependent on Homogeneity

Polymers are classified according on the homogeneity of the repeating units in

1.3.2.1 Homopolymers

Materials made from one monomer are termed homopolymers [17].

1.3.2.2 Copolymers

If their materials made from more than one type of monomer, they are termed copolymers [17].

1.3.2.3 Composite Polymers

Composite polymers involve the addition of material to homogeneous polymers in order to alter some of their properties and introduce new properties [17].

1.3.3 Thermal Classification of Polymers

Polymers are classified according to the effect of temperature

1.3.3.1 Thermoplastic Polymers

The characteristics of these polymers change with the influence of temperature. When the temperature rises, it becomes elastic and sticky. These polymers recover to their original solid state when the temperature is lowered. This is due to the fact that the molecules of a thermoplastic polymer are held together by relatively weak intermolecular forces (Vander Vales forces). Polyethylene, poly vinyl alcohol, Polyacrylamide, and polypropylene are examples of molecules that can slide over each other when heated [18], as shown in figure (1-2).

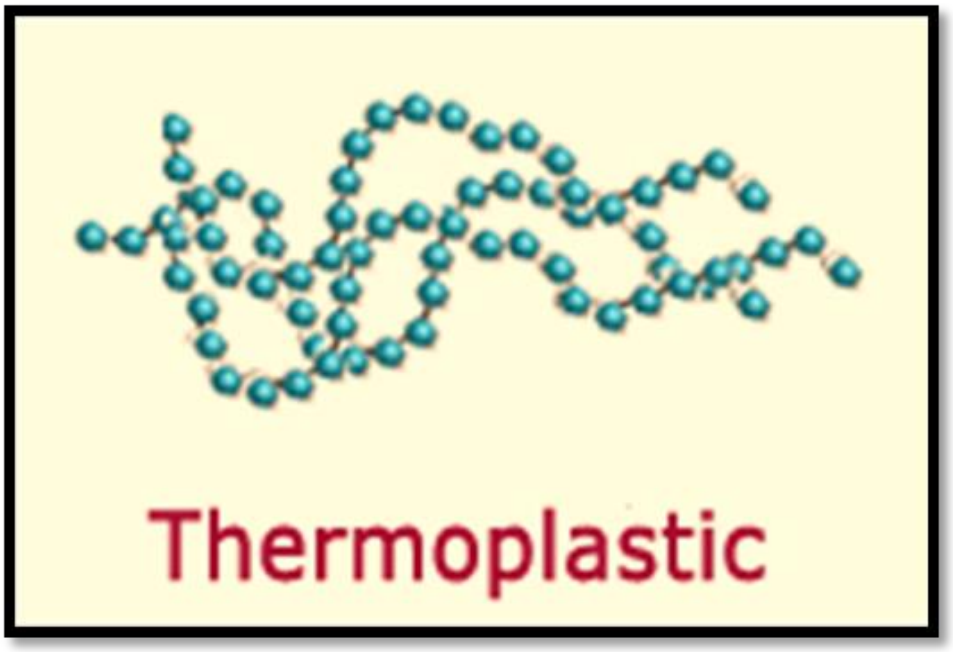

Fig. (1-2) Atomic configuration of thermoplastic polymers [18].

1.3.3.2 Thermoset Polymers

Some polymers undergo certain chemical changes on heating and convert themselves into an infusible mass. The curing or setting process involves chemical reaction leading to further growth and cross linking of the polymer chain molecules and producing giant molecules. For example, resins, Phenolic, epoxy resins, urea , diene rubbers, etc. [18], as shown in figure (1-3).

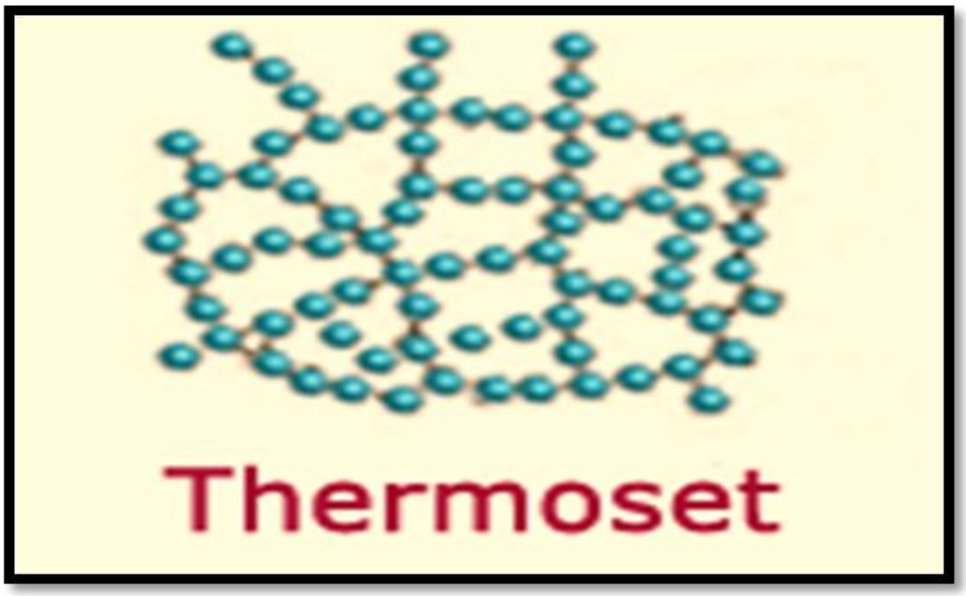

Fig. (1-3) Atomic configuration of thermoset polymers [18].

1.4 Nanomaterials

Nanomaterials are the foundations of nanoscience; they are defined as materials with dimensions less than 100 nm that have at least one unique property that distinguishes them from bulk materials. These properties can be used in a variety of fields, including pharmaceuticals, cosmetics, and nanoelectronics [19]

Nanomaterials are recently produced materials in which the nanoscale structure under control has a significant impact on the material's or device's desired behavior. There are three types of nano-materials: discrete nano-materials, nano-scale device materials, and bulk nano-materials. Discrete nano-materials are those that are individually packaged. Nano-scale device materials are nano-scale material elements that are contained within devices, usual as thin films. Bulk nano-materials are materials with structure controlled at the nano-scale that are accessible in bulk quantity (define here as at least 3 mm volume) [20].

Nanostructures of nano-materials can be classified according to their primary spatial dimensions (X, Y, and Z) [21]

1-zero-dimension (0-D) (represent for quantum dots or nanoparticles)

2-one-dimension (1-D) (indicate to nano-fibres, nano-rods, nano-belts, nano-tubes and nano-wires)

3-two-dimension (2-D) (refer to nano-sheets, nano-walls and nano-plates)

4-three-dimension (3-D) (Nano-flowers and other complex structures, such as nano-tetrapods) are shown in figure (1-4).

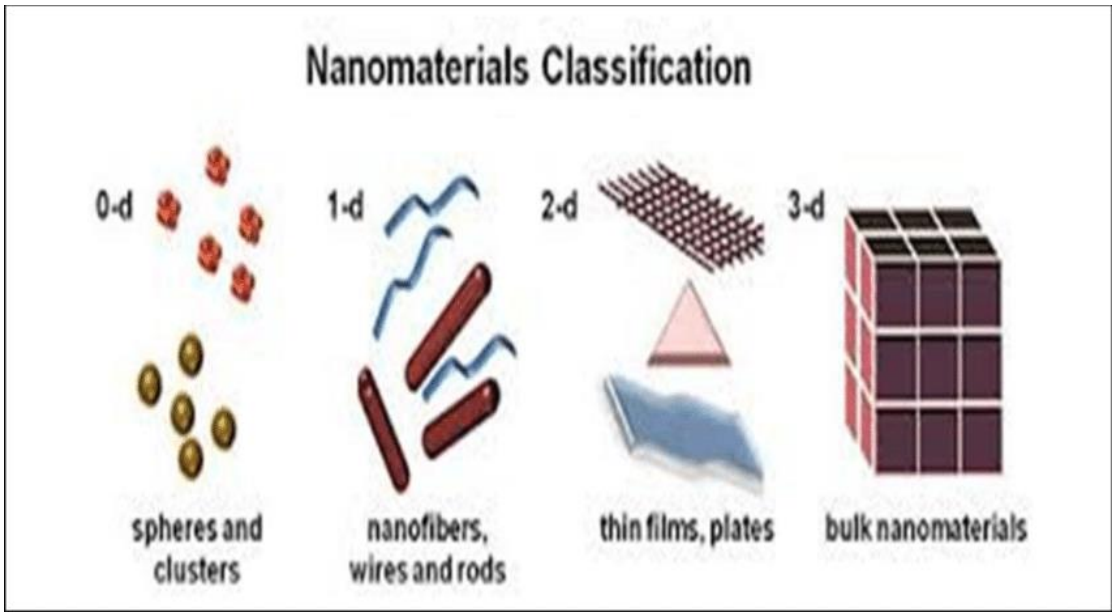

Fig (1-4) Types of nanomaterial[21]

1.5 Nanocomposite

Nanocomposites are a key component in the development of innovative advanced materials for a wide range of applications, including electrical engineering. Nano-composites have piqued the attention of both academia and industry [22]. Since each kind of composite has its own special characteristics and those characteristics may shift from one material to another, a composite's traits are different from those of its constituent parts. The matrix (the fundamental material) and the additives are the two main components of the compound. To build a compact

system, the matrix surrounds other components and makes them more cohesive[23]. Material systems made up of two or more different materials are called composites; the features of a composite are unique from their elements. The matrix (the fundamental ingredient) and the additives are the two main components of the compound. Created by the matrix, this tiny system is held together by other parts[22,23]. The properties of polymer nano-composites are influenced by the nature of the polymer matrix and filler, dispersion state of the particles, filler- matrix interaction, filler size and surface modification of the filler [24].

1.6 The Materials Used in the Study

1.6.1 Poly Methyl Methacrylate (PMMA)

PMMA is one of the oldest and most popular polymers. This material is one of the toughest polymers, a clear glassy with a glossy finish and good weather resistance[25]. PMMA is an important and interesting polymer due to the attractive physical and optical properties crucial to its wide applications. This is a thermoplastic material with good tensile strength and toughness, transparency, good insulation properties and thermal stability[26]. Figure(1-5) show molecular formula of PMMA[27].

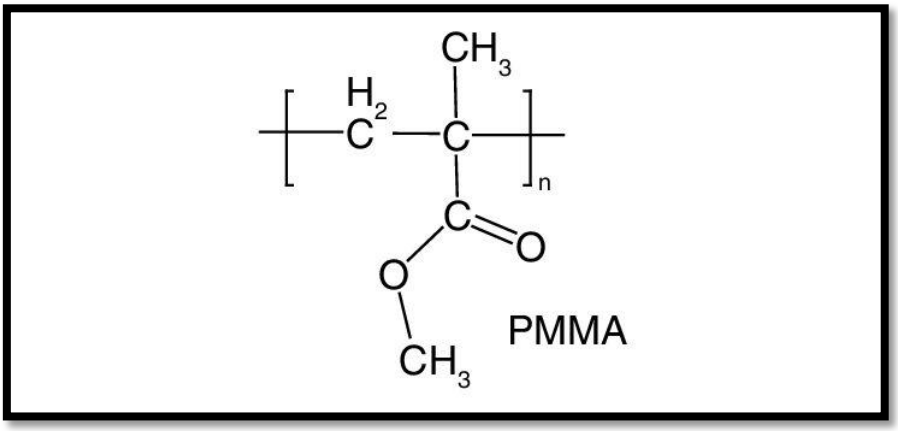

Fig (1-5) Molecular structure of PMMA [27].

Table (1-1) The most important properties of PMMA polymer[28]

Property	Description
Chemical formula	**$CH_2=C(CH_3)COOH_3$**
Tg (^oC)	**106**
Refractive index	**1.49**
Density (g/cm^3)	**1.20**
Melting point (^oC)	**213**
Color	**White**
Linear Thermal Expansion (mm/mm. k)	**6.3×10^5**
Thermal Expansion Coefficient (K^{-1})	**1.80**
Thermal conductivity (W/mK)	**0.12-0.17**
Specific heat (J/Kg. K)	**1466**
Molecular weight (g/mol)	**$(0.1\text{-}0.8)\times 10^6$**

1.6.2. Silicon Nitride (Si_3N_4)

Silicon nitride (Si_3N_4) has been investigated and developed as biomedical implants for orthopedic application since the 1990s, due to its exceptional osteoconductive, biocompatibility and biostability as well as antibacterial activity [29-33]. As an implantable biomaterial with osteogenic bioactivity, Si_3N_4 has been developed for orthopedic devices, such as cages for spinal fusion, component of artificial joints. Previous studies demonstrated that the surface chemistry of SN could change from a silica-rich to a principally silicon-amine composition that might influence the responses of both bacteria and cells/tissues [32]. It was reported that the Si_3N_4 surface possessed inherently resistant to bacteria that could inhibit biofilm formation, indicating excellent antibacterial activity [34]. The antibacterial mechanism of the Si_3N_4 surface is due to the presence of $-NH_2$ group and the formation of a weak alkaline

microenvironment caused by dissolution of Si_3N_4 in the physiological environment [35].

Si_3N_4 ceramics are suitable for the applications which require high loads, wear and corrosion conditions [36]. These are the non-oxides ceramics having the excellent properties of the high melting point, toughness, low density which attracted the applications in several fields. Further, because of high melting point and resistant to wear, Si_3N_4 is considered as the promising ceramic material for the use of the bearings [37]. Si_3N_4 is used in the manufacturing of heat exchangers, turbine blades, bearings, engine components [38]. Table (1-2) explain some physical properties of Si_3N_4 [39,40]

Table (1-2) Some physical properties of Si_3N_4 [39,40]

Property	Description
Chemical formula	**Si_3N_4**
Structure	**hexagonal crystal**
Density (g/cm^3)	**3.44**
Appearance	**grey, odorless powder**
Thermal conductivity (W/m K)	**29.30**
Melting point (^oC)	**1900**
Refractive Index	**2.016**
Resistivity (ρ) (Ω.cm)	**0.60**
Solubility in water	**Insoluble**
Molar mass	**140.283 $g \cdot mol^{-1}$**
Dielectric constant	**7.50**
Coefficient of Thermal Expansion (/°C)	**2810×10^6**

1.6.3 Tantalum Carbide (TaC)

Tantalum Carbide (TaC) is also such a promising ultra-high temperature material [41], it is also shown that TaC is not only wear resistance but it also possesses biocompatible properties appropriate for biomedical applications [42]. The structural, thermodynamic, electronic, and mechanical properties of TaC is also theoretically covered in literature [43-45]. However, to the best of our knowledge, no systematic study on the properties of binary system of TaC has been carried out with which it is likely to introduce new materials with better properties. Tantalum carbide (TaC) is an especially interesting compound among the TMC, as it has some remarkable properties such as high hardness, high melting point [42], resistance to chemical attack and oxidation, catalytic properties and good thermal and excellent electronic conductivity [46-48]. These notable physical and chemical properties can be attributed to the mixed covalent metallic bond [49-51]. Table (1-3) explain some physical properties of TaC [52,53].

Table (1-3) Some physical properties of TaC [52,53].

Property	Description
Chemical formula	**TaC**
Structure	**Face center cubic (FCC)**
Density (g/cm^3)	**14.50**
Molar mass (g/mol)	**192.96**
Appearance	**Brown-gray powder**
Thermal conductivity (W/m K)	**27.90**
Melting point (°C)	**3768**
Boiling point (°C)	**5500**
Refractive Index	**1.70**
Electrical resistivity (Ω.cm)	**0.3030**
Solubility in water	**Insoluble**

1.7 Literature Review

In (2015), Na Sun *et. al.* [54], studied functionalized Si_3N_4 nanoparticles modified with hydrophobic polymer chains by surface-initiated atom transfer radical polymerization (ATRP) method. The ATRP initiators were first immobilized on the surface of Si_3N_4 nanoparticles by using 3-aminopropyl triethoxysilane coupling agent and 2-bromoisobutyryl bromide, and then the polymerization of methylmethacrylate was initiated and propagated on the surface of Si_3N_4 nanoparticles by ATRP reaction. The chemical groups, size, morphology, grafting content, and colloidal thermal stability of PMMA–Si_3N_4 particles were studied by Fourier transform infrared(FTIR),transmission electron microscopy(TEM) and thermo gravimetric analysis(TGA). Results indicate that the grafting of polymer on the surface of Si_3N_4 nanoparticles is successful and the grafting content of PMMA reaches 60.4%. Moreover, the grafted polymer chains have changed the surface properties of Si_3N_4 nanoparticles and enhanced their dispersibility in organic media.

In (2016), S. Natarajan, *et. al*. [55], studied intended to differentiate the antibacterial activities exhibited by PMMA/TiO_2/Ag nanocomposite, towards bacterial consortium and single dominant bacterial isolates from packaged drinking water. A silver nanoparticle dose-dependent decline in cell viability of consortium and individual isolates was compared under UVC and dark conditions to evaluate the antibacterial activity of the nanocomposite. To corroborate with the viability results, oxidative stress & cell permeability was also assessed under similar conditions. Surface characterization of PMMA/TiO_2/Ag nanocomposite was performed by FTIR, AFM, and SEM analyses after interaction with the bacteria. The PMMA/TiO_2/Ag nanocomposite showed enhanced antibacterial activity

against single bacterial isolate compared to the consortium. The outcomes from the study with PMMA/TiO_2/Ag nanocomposite necessitate relooking at the test design for assessment of antibacterial effects in real conditions incorporating the impact on the consortium of microorganisms instead of individual strains.

In (2017), S. Singh, *et. al.* [56], investigated devoted to the performance of the composite films of Barium Titanate ($BaTiO_3$) with Titanium Dioxide (TiO_2) and Poly (methyl methacrylate) (PMMA) by simple solution casting technique. From the X-ray diffraction (XRD), The average crystallite size of the $BaTiO_3$ particles in the composite films has been found to be lies in between ~ 20 -70 nm. It has been found that the peak intensities increase with increasing the wt.% of $BaTiO_3$ in the composite films at room temperature (RT). The XRD analysis revealed that the addition of TiO_2 has played a crucial role to enhance the crystalline nature of the composite films at room temperature. Efforts have been made to correlate the results with investigated XRD results of pure $BaTiO_3$ and its composites as observed by other workers at room temperature.

In (2018) G. Soni *et al*. [57], fabricated thin films composed of PMMA polymer doped with SiO_2, with a thickness of 60 microns using the solution casting method, then they tested the effect of adding nanoparticles on the electrical and structural properties of the thin films. The optical band gap it was observed that it decreased with increasing concentration of SiO_2 nanoparticles.

In (2019) D. Nayak and R. B. Choudhary [58], studied the optical and electrical properties of PMMA-ZnS nanocomposite. The morphological structure indicated that the nanocomposite was well mixed. For the optical properties observed that the energy gap got to a

low value (~3.30) with increasing concentrations of ZnS. The dielectric properties of PMMA-ZnS showed a high dielectric constant and high electrical conductivity with increasing the frequency. The high value of the singlet constant and the decrease in the optical band gap with increasing conductivity confirmed that it could be used of PMMA-ZnS nanocomposite as an emissive layer in OLED devices.

In (2020), G. Soni *et. al.* [59], have studied the effect of a mixture of ZnO and SiO_2 nanoparticles on the optical properties of the composite thin film PMMA/ZnO/SiO_2, with a thickness of 50 μm by solution casting method and they observed that the optical band gap of the composite thin films decreases with increasing concentration of zinc oxide and silica.

In (2020) Yang *et. al.* [60], designed and arranged the poly(methyl methacrylate) (PMMA)/polystyrene (PS) and PMMA fibers artificially, porous PMMA templates with different coding orders (e.g. "1 × 1", "3 × 3", "5 × 5", and "7 × 7") are created after multi-step drawing followed by the dissolution of the inner PS. With these templates, coding arrays of CuMWs with diameters of 2–10 μm are fabricated. The geometries of the obtained templates and CuMWs arrays are shown to be consistent with the design values. This new approach extends the types and quality of CuMWs and makes it possible to devise extremely complex array structures with micro or even nano dimensions for diverse optical applications such as spectral sensing, laser phased arrays, and photonic crystal fibers.

In (2021), Xinglong Hu *et. al.* [61], studied a microporous surface containing both Si_3N_4 and Ta microparticles on polyetherketoneketone PEKK exhibiting excellent osteogenic and antibacterial activity was created by sulfonation. Compared with sulfonated PEKK without

microparticles, the surface properties (roughness, surface energy, hydrophilicity and protein adsorption) of STP significantly increased due to the Si_3N_4 and Ta particles presence on the microporous surface. In addition, PEKK also exhibited outstanding antibacterial activity, which inhibited bacterial growth *in vitro* and prevented bacterial infection *in vivo* because of the presence of Si_3N_4 particles. Moreover, the microporous surface of PEKK containing both Si_3N_4 and Ta particles remarkably induced response (e.g., proliferation and differentiation) of rat bone mesenchymal stem (rBMS) cells *in vitro*. Therefore, PEKK possessed the dual biofunctions of excellent osteogenic and antibacterial activity, showing great potential as a bone substitute.

In (2022), Q. A. Alsulami and A. Rajeh [62], employed the casting method for the preparation of polymer blend films doped with TiO_2 (0.5, 1, 1.5, and 2.3 wt%). The TiO_2 phase formation is anatase, with an average crystal size of 20.25 nm, according to the XRD results. The samples of PANI/PMMA-TiO_2 nanocomposite are amorphous nature. The FTIR technique is used to reveal the nanocomposites' vibrational bands as well as the intermolecular bonding between the blend and the TiO_2 NPs. Absorption spectra, reflectance, transmission spectra, extinction coefficient, refractive index, real and imaginary parts of the dielectric constant, third-order susceptibility ($\chi 3$), and optical band gaps are among the optical constants studied. As preselected TiO_2 NPs are put into thin films (doping $\leq$1.5 wt%), the optical band gap values (Eg) of the fabricated nanocomposite films decreased. The optical constants revealed noticeable changes with increasing doping concentrations; according to the experimental data. The doped thin films that were developed have a great promise for manufacturing high-efficiency optoelectronic devices.

1.8 Aims of Project

Aims of this work can be summarized:

1- Preparation of the PMMA/Si_3N_4/TaC nanocomposites by using casting method with high homogenous.

2- Studying the effect of the Si_3N_4 and TaC nanoparticle on the structural, optical, and A.C electrical properties of PMMA polymer.

3- Study the antibacterial activity of the application of PMMA/Si_3N_4/TaC nanocomposites.

Chapter Two

Theoretical part

2.1 Introduction

This chapter includes a general description of the study's theoretical part, including physical concepts, relationships, scientific clarifications, and laws applied to explain the study's findings.

2.2 Structural and Morphological Properties

2.2.1 Optical Microscope (OM)

A compound optical microscope is an optical tool that magnifies an object (or specimen) and projects it onto the retina of the eye or onto an imaging device using visible light. The term "compound" refers to how two lenses, the objective lens and the eyepiece (or ocular), work together to generate the image's final magnification.

Both diffracted (rays that interact with the specimen) and non-diffracted (rays that pass through the specimen without deviating) rays are gathered by the objective lens in most kinds of transmitted light microscopy and contribute to picture generation [67].

2.2.2 Fourier Transforms Infrared Ray (FT-IR)

Chemical analytical spectroscopy is Fourier transforms infrared (FTIR). It tests the sensitivity of infrared with the number of light waves. The wavenumbers consist of infrared light classified into three zones, far-infrared, mid-infrared and near-infrared, ranging from (4 ~ 400) cm^{-1}, (400 ~ 4000) cm^{-1} and (4000 ~ 14000) cm^{-1}, respectively. The allowable use of this technology depends on detecting the vibration of the chemical functional group in a sample. Where, as the contact takes place between the infrared light and the substance, the chemical bonds will stretch. Here, independent of the rest of the molecule composition, the infrared addition is captured by the chemical functional group at a particular wavenumber range, More complex molecules contain more than one bond [65].

The idea behind this method is that chemical bonds vibrate at various frequencies. FTIR spectroscopy is a powerful tool for identifying different types of chemical bonds in a molecule by creating a molecular "fingerprint" in the form of an infrared absorption spectrum. Molecular bonds vibrate at different frequencies depending on the components and the type of interaction. FTIR may be used to identify unknown compounds, detect organic and inorganic additives at low levels, and analyze chemical structure change and solvent residue since it can reveal information about a material's chemical bonding or molecular structure without damaging [66].

2.2.3 Field Emission Scanning Electron Microscopy (SEM)

A significant method for investigating the surface and morphology of nanostructures is scanning electron microscopy (FE-SEM). By using it, we can estimate the nanostructure 's diameter, weight, thickness, density, shape and orientation [63]. To emit electrons by heating, an electron gun made of tungsten or LaB-6 filament is used and these emitted electrons are guided and concentrated on the sample by the use of an anode and various electromagnetic lenses between the electron gun and the sample. After entering the sample, these predicted electrons expel secondary and back-scattered electrons. These secondary and back scattered electrons expelled from the sample are detected by detectors and these detectors pass these electrons detected into the electronic signal sent to the image display device, as shown in figure (2-1) [64].

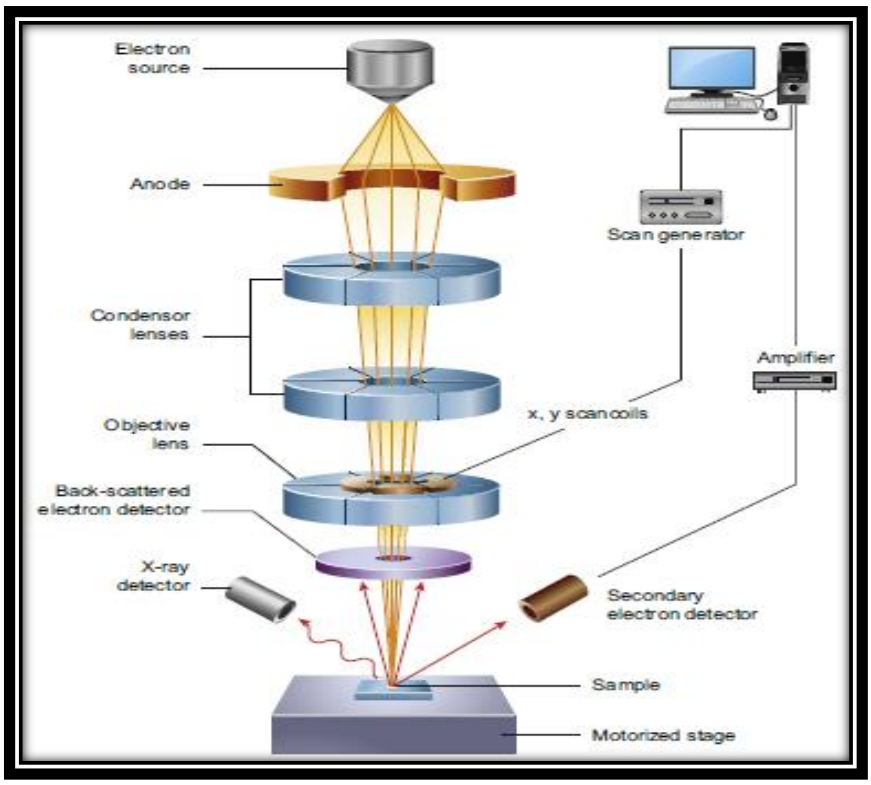

Fig.(2-1) Schematic diagram of the field emission scanning electron microscopy[64].

2.3 Optical Properties

The basic absorption mechanism for incident rays in crystalline semiconductors occurs when an electron in the valance band absorbs high energy from the incident photon to escape to the conduction band if the energy of the photon (h*v*) is equal to or greater than the forbidden energy gap (E_g)[68].

$$E_g \geq hv \qquad (2-1)$$

Where (h*v*) Plank's constant ($6.625x10^{-34}$ J.s) and ν is the frequency in (Hz). Spectroscopy of the region of incident rays that start transporting electrons is called (fundamental absorption edge).

2.3.1 The Fundamental Absorption Edge

The basic absorption edge is a sudden increase in absorbance that occurs when the amount of absorbed energy radiation is about equal to

the band energy gap; As a result, the basic absorption edge shows the energy differential between the up point of the valance band and the bottom point of the conduction band. Figure (2.2) shows three types of absorption zones [69].

A. High absorption region

Magnitude (α) in the part A is greater than or equal to $10^4 cm^{-1}$. The magnitude of the prohibited optical band gap (E_g^{opt}) can be introduced from this area.

B. Exponential region

The value of (α) in component B is in the range $1\ cm^{-1} < \alpha < 10^4\ cm^{-1}$. It refers to the transition from extended levels at the top of the valence band to localized levels in the conductive band and vice versa, from local levels in (V.B.) to extended levels at the bottom of the conductive band and vice versa (C.B).

C. Low Absorption Region

Value of (α) in component C is relatively tiny. it's around $\alpha < 1cm^{-1}$. The transition happens in this area as a result of structural faults causing state density inside space motion [70].

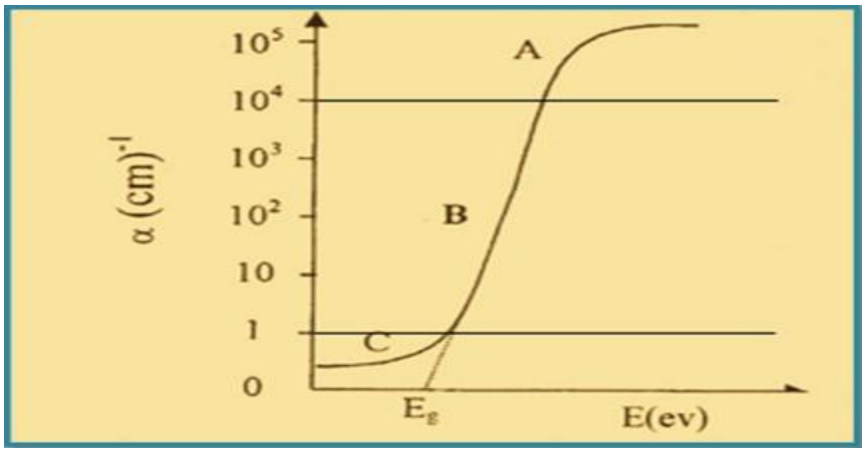

Fig. (2-2) Absorption edge variation with absorption regions [65]

This phase occurs when the width of the forbidden energy gap is equal to the incident energy photon that can be expressed in equation (2-1) [71]. when (Eg =hν$_o$) is called the critical frequency and the wavelength facing it is called the wavelength cut off (λc).

$$\lambda(\mu m) = \frac{hc}{Eg} = \frac{1.24}{Eg(eV)} \qquad (2\text{-}2)$$

Where (c) is the speed of light in vacuum.

2.3.2The Electronic Transitions

The electronic transformations can essentially be divided into two types [72]:

2.3.2.1 Direct Transitions

This transition occurs in semiconductors when the conductive bottom (C.B) is exactly above the valence band (V.B). This means they have the same wave vector value (ΔK=0); the absorption occurs in this state when (Eg = hν). This form of transition involves the laws of energy and momentum conservation. There are two forms of direct transformations, these are [73]:

a) Allowed Direct Transition

Fig.(2-3-a) shows that this transition occurs from the top points in the (V.B) and the bottom point in the (C.B). The equation (2-3) provides the Tauc empirical relationship for this type of transition [74]:

$$\alpha h\upsilon \approx \left[h\upsilon - E_g\right]^{1/2} \qquad (2\text{-}3)$$

b) Forbidden Direct Transition

The transition from near the top points of (V.B) and the bottom points of (C.B) is shown in Fig.(2-3-b). The equation (2-4) gives the empirical relationship that corresponds to this transition [75]:

$$\alpha h\upsilon \approx \left[h\upsilon - E_g\right]^{3/2} \qquad (2\text{-}4)$$

2.3.2.2 Indirect Transitions

When the bottom of (C.B) is not above the top of (V.B), in the curve (E-K), this transformation occurs. Where the value of the electron wave vector before and after transition is not equal ($\Delta K \neq 0$), the electron transits from (V.B) are not perpendicular. This form of transformation happens with the aid of a related particle called "Phonon," for energy and momentum law conservation. Hence, a phonon 's support is required to maintain the momentum,[75]:

$$h\nu = E_g \pm E_P \quad (2\text{-}5)$$

$$hk_f = hk_i \pm hk_p \quad (2\text{-}6)$$

Where the strength of the absorbed or emitted phonon is E_p.

c) Allowed Indirect Transitions

Fig.(2-3-c) indicates the change between the top of (C.B) and the bottom of (V.B) located in the area of (K-space) gap, so that [75]:

$$\alpha h\upsilon \approx \left(h\upsilon - E_g\right)^2 \quad (2\text{-}7)$$

d) Forbidden Indirect Transitions

Fig.(2-3-d) indicates that this transition occurs between close points at the top of (C.B) and close points at the bottom of (V.B). The absorption coefficient for the phonon on-absorption transition is defined by the following equation [76]:

$$\alpha h\upsilon \approx \left(h\upsilon - E_g\right)^3 \quad (2\text{-}8)$$

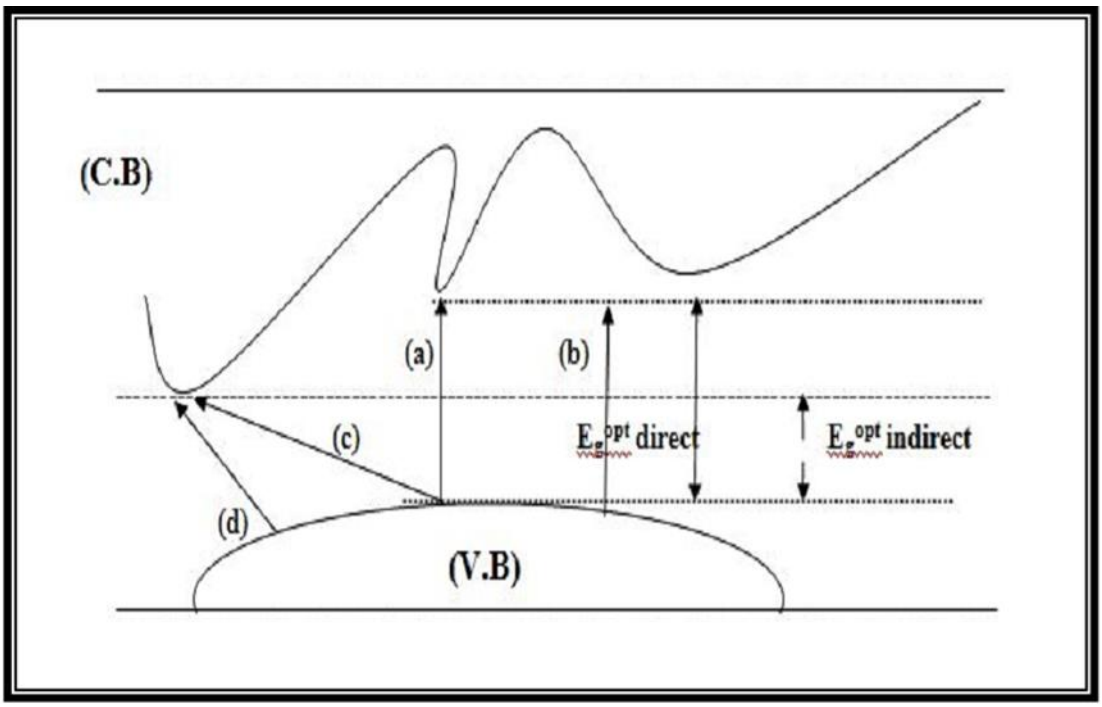

Fig.(2-3) The types of transitions [75]
(a) allowed Direct, (b) forbidden Direct,
(c) allowed Indirect, (d) forbidden Indirect.

2.3.3 Optical Constants

Optical constants are parameters which are very important since they explain the materials' optical behavior. An area of common interest [76] is the extraction of optical constants from various methods of optical measurement. The refractive index (n), extinction coefficient (k_o), real (ε_r) and imaginary (ε_i) parts of the dielectric constant were included in the optical constants [77].

$$n = \left(\frac{4R}{(R-1)^2} - ko^2\right)^{1/2} + \frac{(R+1)}{(R-1)} \qquad (2\text{-}9)$$

Where the reflectance is (R)

The extinction coefficient (k_o) is associated with the wave's exponential decay as it passes through the medium, and is defined as [78]:

$$k_o = \frac{\alpha\lambda}{4\pi} \qquad (2\text{-}10)$$

where (λ) is the incident radiation wavelength and (α) is given by[78].

$$\alpha = 2.303\frac{A}{t} \qquad (2\text{-}11)$$

(A) is absorbance, and (t) is thickness of sample and (R) was calculated from the following equation [78].

$$R+T+A=1 \quad (2\text{-}12)$$

Where the (T) is the transmittance was calcilated from the following equation[79]:

$$A= -\log_{10} T \quad (2\text{-}13)$$

The real part (ε_r) and imaginary part (ε_i) of dielectric constant can be calculated by using the following equation [79].

$$(n - ik)^2 = \varepsilon_r - i\,\varepsilon_i \quad (2\text{-}14)$$

The real and imaginary dielectric coefficient can be written as in following equation [79].

$$\varepsilon_r = n^2 - k^2 \quad (2\text{-}15)$$

$$\varepsilon_i = 2nk \quad (2\text{-}16)$$

The optical conductivity (σ_{op}) depends directly on the refractive index (n) and absorption coefficient (α) by the following relation [79].

$$\sigma_{op} = \alpha\, n\, c/4\pi \quad (2\text{-}17)$$

c is the speed of light, α is the absorption coefficient.

2.4 Electrical Properties

The electrical properties of the material depend on the chemical composition, the arrangement of atoms in the solid and the presence of defects in the energy gap. In several ways, such as the annealing, this defect can be reduced. The electrical properties are also highly dependent on the preparation technique and the deposition conditions [80].

Matter can be classified according to its electrical conductivity into insulators, semiconductors and conductors. Conductivities for some

polymers are (~ 10^{-17} Ω^{-1} cm^{-1}) for polyethylene, (10^{-16} Ω^{-1} cm^{-1}) for polystyrene and (10^{-12} Ω^{-1} cm^{-1}) for polyamides. The electrical properties are designed to understand the number, origins, and actions of a charge. This includes the exact composition of the substance, the chemical composition, and the shape of the substance [81].

2.5 The Electrical Polarization

Electric polarization is a phenomena that occurs when the centers of negative and positive charges don't coincide. When an electric field is applied to a dielectric material, this phenomenon usually appears. Because an electric field is applied during electrical resistivity measurements, polarization in a material can happen during electrical resistivity measurements [82]. It's worth noting that this polarized surface charge density (formerly represented by (P) and also referred to as simply polarization or induced polarization) is perfectly equal to the value of the dipole moment for each unit volume [82].

$$P = N_m \mu \qquad (2\text{-}18)$$

Where : N_m is the number of molecules. We can make the following assumption about the dipole moment being proportion to the electrical field [83].

$$\mu = a_o \ E \qquad (2\text{-}19)$$

where a_o: is a constant named the polarizability, E: is an electrical field intensity. The relation between the electrical displacement (flux density) (D) and (E) is shown by [84].

$$D_o = \varepsilon_o E \qquad (2\text{-}20)$$

where: $\varepsilon_o = 8.854 \times 10^{-12} F/m$ is the permittivity of a vacuum.

The electric flux density in the dielectric part is proportional to that in vacuum by [85].

$$D = \varepsilon_o E + P \quad (2\text{-}21)$$

As:

$$D = \varepsilon' \varepsilon_o E \quad (2\text{-}22)$$

But, $\varepsilon' = D / \varepsilon_o E$

Then:

$$\varepsilon' = 1 + P/(\varepsilon_o E) \quad (2\text{-}23)$$

The polarizability and dielectric constant are related by the Clausius-Mossotti equation [83].

$$(N_m a_o)/(3\varepsilon_o) = (\varepsilon' - 1)/(\varepsilon' + 2) \quad (2\text{-}24)$$

Polarization of material can be detected by the components of this polarization so that the total polarization can be calculated, figure (2-4) depicts the several types of polarization [86].

$$P = P_e + P_i + P_d + P_o \quad (2\text{-}25)$$

A- Electronic Polarization (P_e)

Electronic polarization arises as a result of a distortion in the charge distribution caused by an external electric field. A separation arises between the positive charge of the nucleus and the center of the negative charge, resulting in the generation of induced dipoles [87]. Electronic polarization occurs in a relatively short period of time (10^{-15} seconds) and is not affected by temperature [88], as shown in figure 1. (2-4-a).

B- Ionic Polarization (P_i)

It was generated as an ionic compound with ionic properties. It occurred when matter was subjected to an electric field, which altered the lengths of the ionic bonds, resulting in the formation of a net dipole moment in the molecule that did not exist previously [87]. It only lasts for about 10^{-11}–10^{-13} seconds [88]. The temperature has no effect on this type of polarization, as showed in the figure (2-4-b).

C- Rotational or Orientation Polarization (P_d)

It's also called as molecular polarization. This occurs in molecules with a perpetual dipole moment [89]. When the electric field is applied, the dipoles revolve around of the axis , also arrange themselves in direction of the field. This type of polarization is dependent on temperature and takes a long time to occur [87], as showed in the figure (2-4-c).

D- Space Charge or Interfacial Polarization (P_o)

It occurs when a matter contains impurities, a vacuum, or a structural fault, which results in a concentration of opposing charges on the impurities terminals, this refers to the formation of dipoles within an molecule ,atom, or zone of material. This type of polarization is dependent on homogeneity of matter and the rate of being free from impurities. It occurs mostly in radios frequency and can be expand to frequencies beneath audio and depending on flaws that produces the polarization [87], as illustrated in figure (2-4-d).

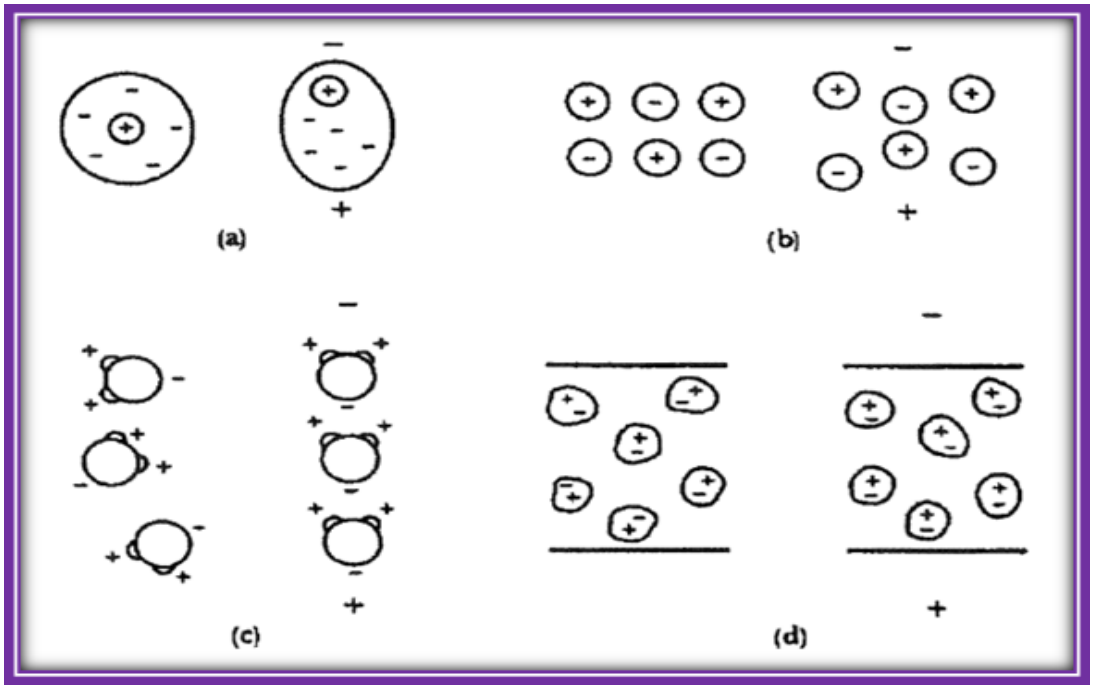

Fig. (2-4) Four different types of polarization [86]

a: Electronic polarization c: Orientation polarization d: Space charge b: Ionic polarization

2.5 The A.C Electrical Conductivity

A.C conductivity affects the frequency of the electrical field [90]. Dielectric spectroscopy is based on the calculation of current and voltage phases and the amplitude A.C system. It is commonly used for the study of dielectric properties of polymers e.g. (ε', tan δ) [91]. The electrical conductivity of isolation polymer materials can be improved through adding certain conductive fillers [92]. The dielectric constant represents the ratio of the capacitance of the condenser that contains an insulator material between its conductive plates, to the capacity of the same size but with vacuum between its plates. Its value varies from material to material based on the amount of polarization that occurs in the material [93]. When an alternating potential $V = V_m e^{i\omega t}$ [93] is applied through a capacitor (C) loaded with an insulator, the current going through the capacitor will precede the potential by π/2 [94].

$$I = j\omega c v_m \qquad (2\text{-}26)$$

Where (ω) is the applied angular frequency of the filed (ω=2πf), (j) refers to the number of imaginary and is equal to $\sqrt{-1}$, (C) is the capacitance of a capacitor, and (V_m) is the highest voltage. The angle between electric current and voltage is less than π/2, as seen in Figure (2.4). The sum of the conduction current (I_p) is assumed to be electric current. This is in the same phase with voltage, whereas the capacitates current (I_q) is with the phase variation (π/2). The current can be obtained through the equation below [94].

$$I = I_P + jI_q \qquad (2\text{-}27)$$

The capacitance of a condenser consisting of two parallel plates can be defined through the following equation [95].

$$C = \frac{A_r}{d}\varepsilon \qquad (2\text{-}28)$$

where (A_r) is the area of the sample, and (d) is the thickness of sample.

By substituting equation (2.27) in (2.28), the following relation is obtained:

$$I = i\,\omega\,\varepsilon\,\varepsilon_o V\,A_r/d \qquad (2\text{-}29)$$

The dielectric constant is then viewed as a complex quantity (ε). The difference of the real and imaginary components of the complex dielectric constant is defined as follows [96].

$$\varepsilon = \varepsilon' - i\,\varepsilon'' \qquad (2\text{-}30)$$

where (ε") is the dielectric loss.

$$I = i\,\omega\varepsilon_o \frac{A_r}{d}(\varepsilon' - i\,\varepsilon'')\,V \qquad (2\text{-}31)$$

By comparing equation (2.27) to (2.31), the following can be obtained:

$$I_p = \omega\varepsilon_o \varepsilon'' \frac{A_r}{d} V \quad (2\text{-}32)$$

$$I_q = \omega\varepsilon_o \varepsilon' \frac{A_r}{d} V \quad (2\text{-}33)$$

Figure (2-5) shows that the loss factor (tan δ) is calculated by the following equation [94].

$$\text{Tan } \delta = I_p / I_q = \varepsilon''/ \varepsilon' \quad (2\text{-}34)$$

The capacitor can be represented by an ideal capacitor connected in parallel with a resistance R_P at low frequencies, so:

$$I = I_p + iI_q = \frac{V}{R_P} + i\,\omega C_p V \quad (2\text{-}35)$$

Hence, the impedance **z** is then given by

$$\frac{1}{Z} = \frac{1}{R_P} + i\,\omega\, C_p \quad (2\text{-}36)$$

From equations (2-32), (2-33) and (2-35), one can write [94].

$$R_P = d / \omega A_r \varepsilon_o \varepsilon'' \quad (2\text{-}37)$$

$$\varepsilon'' = 1 / \omega R_P C_o \quad (2\text{-}38)$$

$$C_P = \varepsilon_o \varepsilon' A_r /d \quad (2\text{-}39)$$

$$\varepsilon' = C_P / C_o \quad (2\text{-}40)$$

The dissipated power in the insulator is represented by the existence of alternating potential as a function of the alternating conductivity, as explained in the following equation [95]:

$$\sigma_{A.C} = \omega\, \varepsilon_o\, \varepsilon'' \quad (2\text{-}41)$$

$\sigma_{A.C}$ represents the measurement of the temperature produced by the insulation material arising from the vibration of the charges or rotation of the dipoles in their positions. This is the result of the alternation of the field [97].

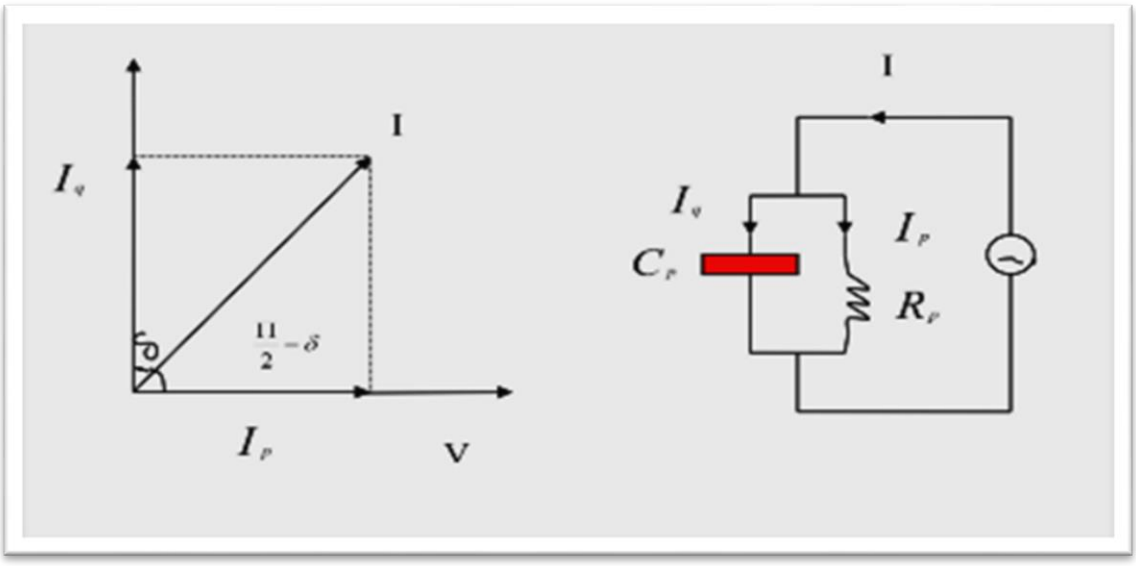

Fig. (2-5) The circuit equivalent to non-ideal capacitor [84].

2.6 Antibacterial Mechanisms of Nanoparticles

NPs must come into touch with bacterial cells in order to perform their antimicrobial effect. Electrostatic attraction, van der -Waals forces, receptor ligand interactions, finally hydrophobic interactions. NPs enter the bacterial membrane and aggregate throughout the metabolic route, altering the cell membrane's shape and function. The NPs then interact with DNA, lysosomes, ribosomes, and enzymes in the bacterial cell, causing oxidative stress, heterogeneous modifications, changes in cell membrane permeability, electrolyte balance issues, enzyme inhibition, protein deactivation, and gene expression changes [98].

The most important mechanism of nanoparticles toxicity to bacteria is damage to cell membrane, besides cell membrane damage, generation of reactive oxygen species, disturbance in metal/metal ion homeostasis, protein and enzyme dysfunction and geno-toxicity [99].

2.6.1 Bacterial Strain

1. *Staphylococcus aureus (S. aureus)*

Staphylococci are gram-positive bacteria that have individual cocci that separate in several planes to form grape-like clusters. They are

often non-motile and do not produce spores [100]. S. aureus are facultative anaerobes that can grow by aerobic respiration or fermentation and can grow at temperatures ranging from 15 to 45 °C and at NaCl concentrations as high as 15%. The hard protective layer, (microbial surface components recognizing adhesive matrix molecules) produced on the surface of S. aureus boosted antibiotic resistance and boosted the bacteria's adherence to host proteins such as fibronectin and fibrinogen. *S. aureus* is considered to be a major pathogen that colonizes and infects both hospitalized patients with decreased immunity, and healthy immuno-competent people in the community [101].

2. *Klebsiella aerogenes (K. aerogenes)*

Klebsiella aerogenes is an important cause of bacteremia in patients whose immunity is impaired by disease, trauma or immunosuppressive drugs. The mortality associated with these infections suggests that contemporary antimicrobial therapy could be improved. Clinical trials have shown that passive immunotherapy can halve the mortality of patients susceptible to Gram-negative bacteremia. In these trials the protective antibodies were raised in human volunteers to Escherichia coli OIII: B4 15 and attributed to a part of the lipopolysaccharide on the surface of the bacteria known as 'core-glycolipid' which is highly conserved in all species of Gram-negative bacteria [102].

Chapter Three

Experimental Part

3.1 Introduction

This chapter includes the preparation process, instrumentation, and measurement techniques. A general description of materials (Poly methacrylate (PMMA), Silicon Nitrite (Si_3N_4) and Tantalum Carbide (TaC)) used in this work are given by Optical Microscope (OM), Fourier Infrared Transform Spectrometer (FT-IR), Scanning Electron Microscope (SEM), AC electrical properties and application for antibacterial activity.

3.2 The Used Materials

The substances used in this research are:

3.2.1 Matrix Material

Poly Methyl Methacrylate (PMMA): The polymer is used as granular form and could be obtained from local markets, white colors and high purity (99.99 %).

3.2.2 Additive materials

1. Silicon Nitrite (Si_3N_4): nanoparticles: It was obtained as powder form and could be obtained from local markets, with radius 30 nm**,** white powder and high purity (99.999 %).

2. Tantalum Carbide (TaC): nanoparticles: It was obtained as powder form and could be obtained from local markets, with radius 50 nm, grey-odorless powder and high purity (99.999 %).

3.3 Preparation of Nanocomposites

The (PMMA/Si_3N_4/TaC) nanocomposites are prepared by the following:

1. Nanocomposite films have been prepared by mixing dissolving 1.5 g of PMMA in 30 ml of chloroform at room temperature with magnetic stirrer for 1.5 h to obtain more homogenous solution.

2. Adding the weight percentages of additives (2, 4, 6, and 8) wt.% of (Si_3N_4/TaC) nanoparticles we get the films from this mixture using the casting process, which involves placing the mixture in a template (Petri dish has a diameter of 9cm), and then left for one days to dry mixture, then taken from template quietly to conducting the necessary tests, using micrometer to measure thickness and found the thickness about (22 μm).

3- Fig. (3-1) shows the preparation condition of (PMMA/Si_3N_4/TaC) films and the structural, electrical, optical measurements and antibacterial application.

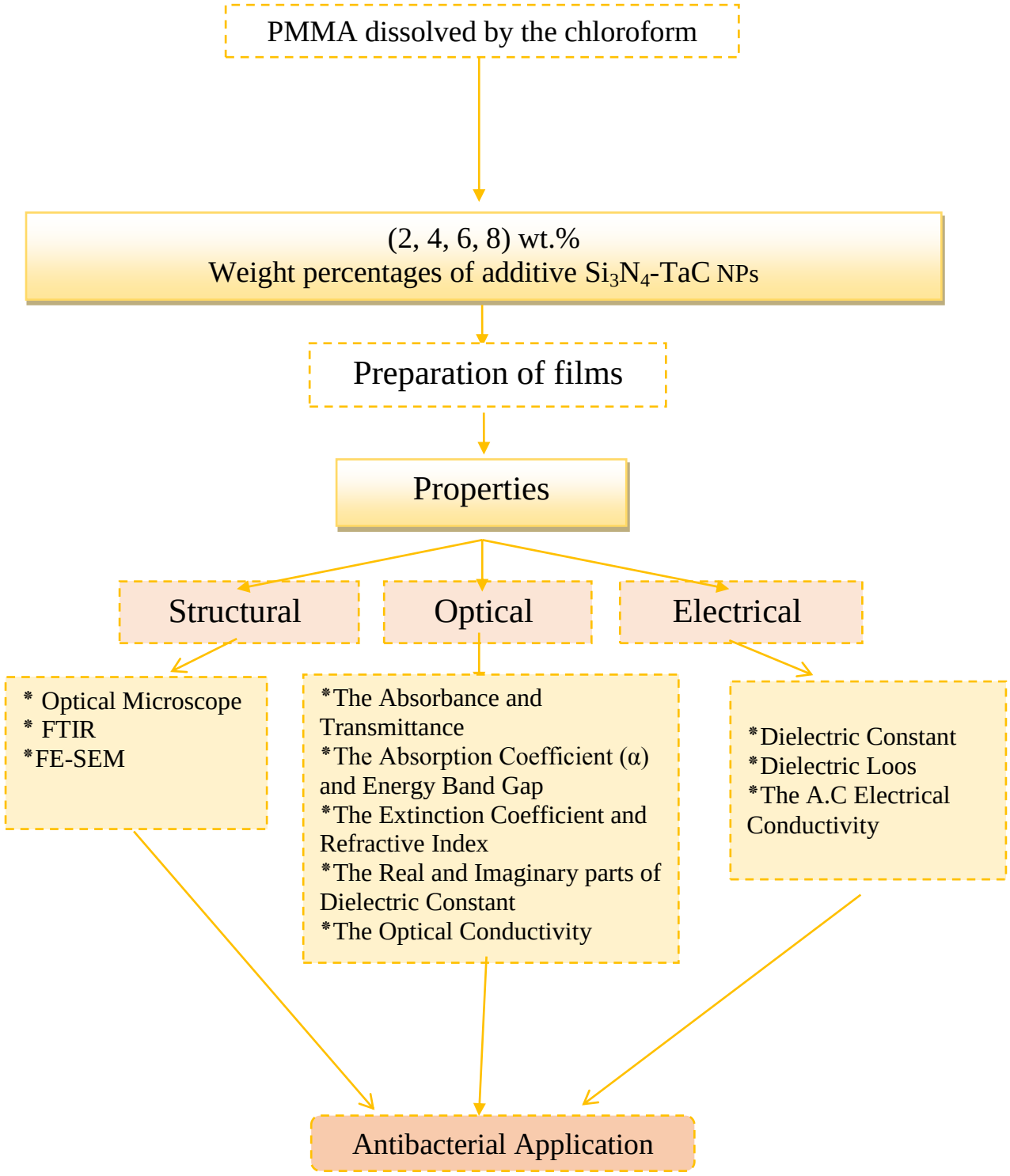

Fig. (3-1) Schematic diagram of experimental work.

3.4 Measurements of Structural Properties

3.4.1 Optical Microscope

The (PMMA/Si_3N_4/TaC) nanocomposite films are analyzed using the optical microscope, which was supplied from Olympus name (Top View) type (Nikon-73346), equipped with light intensity automatic controlled camera under magnification (40x), as shown in figure (3-2), it is implemented in the university of Babylon /college of education for pure sciences/ department of physics.

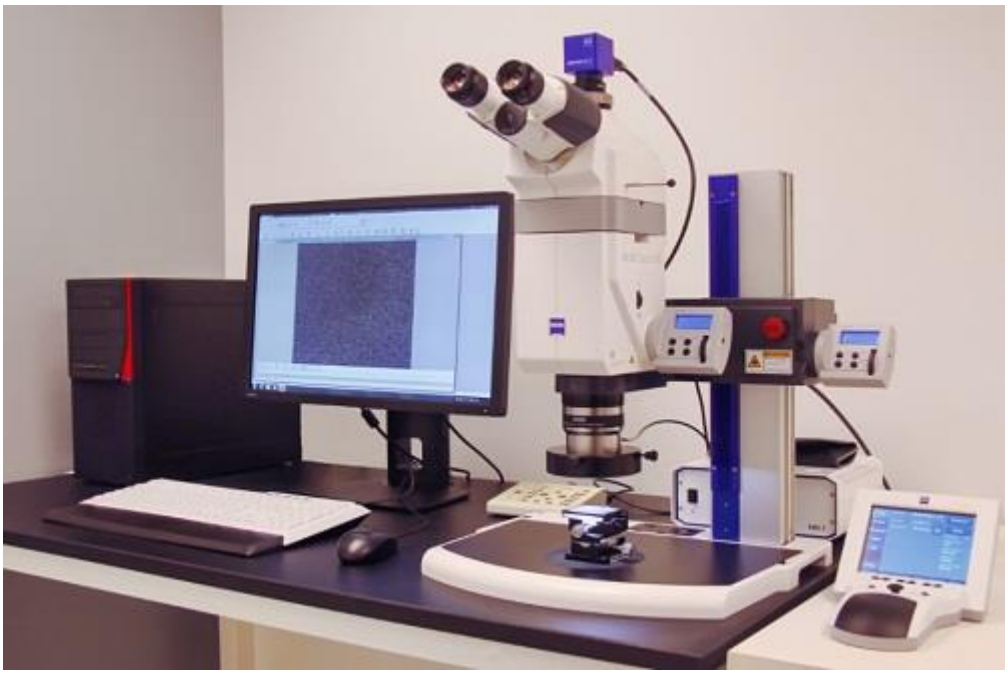

Fig. (3- 2) Optical Microscope

3.4.2 Spectral Characterization for FT- IR

FTIR spectra were recorded by FTIR Bruker company, German origin, type vertex -70. The spectrum of wave numbers considered is (500-4000) cm^{-1}, as shown in figure (3-3). FTIR has been introduced in the university of Babylon /college of education for pure sciences/ department of physics.

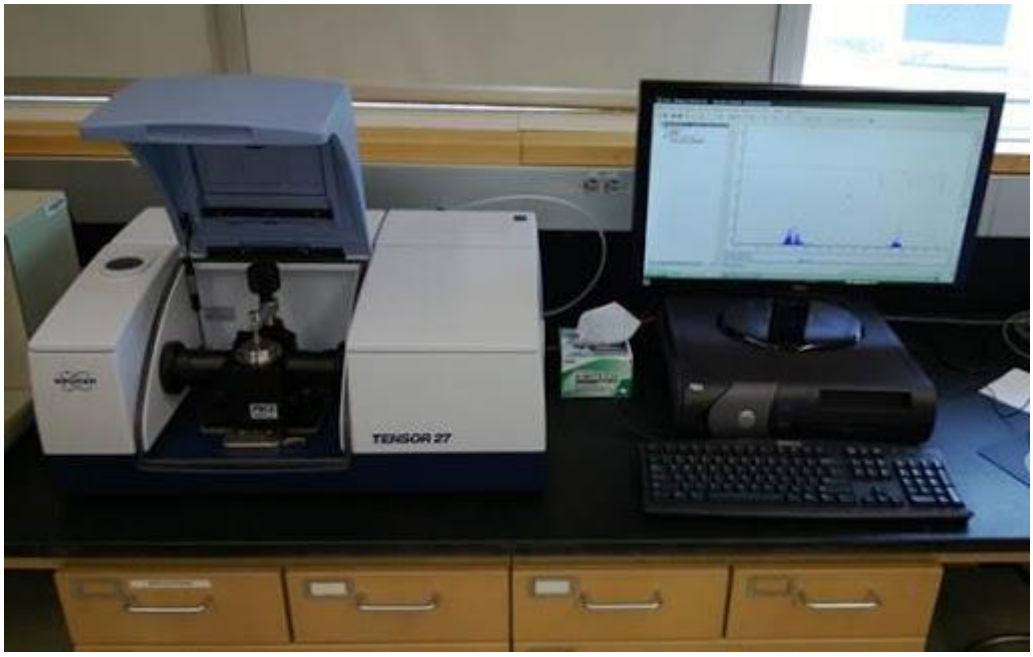

Fig. (3-3) FT-IR spectroscopy

3.4.3 Field Emission Scanning Electron Microscope (FE-SEM)

A centered beam of electrons is sent onto the sample in scanning electron microscopy. In the sample, the primary electrons communicate with atoms, generating different signals that can be observed and contain information about the surface topography and structure of the sample. In general, the electron beam is scanned in a raster scan pattern, and the direction of the beam is coupled with the observed signal to create an image where the electrons are distributed through the sample in the primary beam, SEM creates images by sensing secondary electrons released from the surface due to the primary electron beam excitation accompanied by elastic scattering processes, as shown in figure (3-4). The examination was carried out in the laboratory of the university of Tehran.

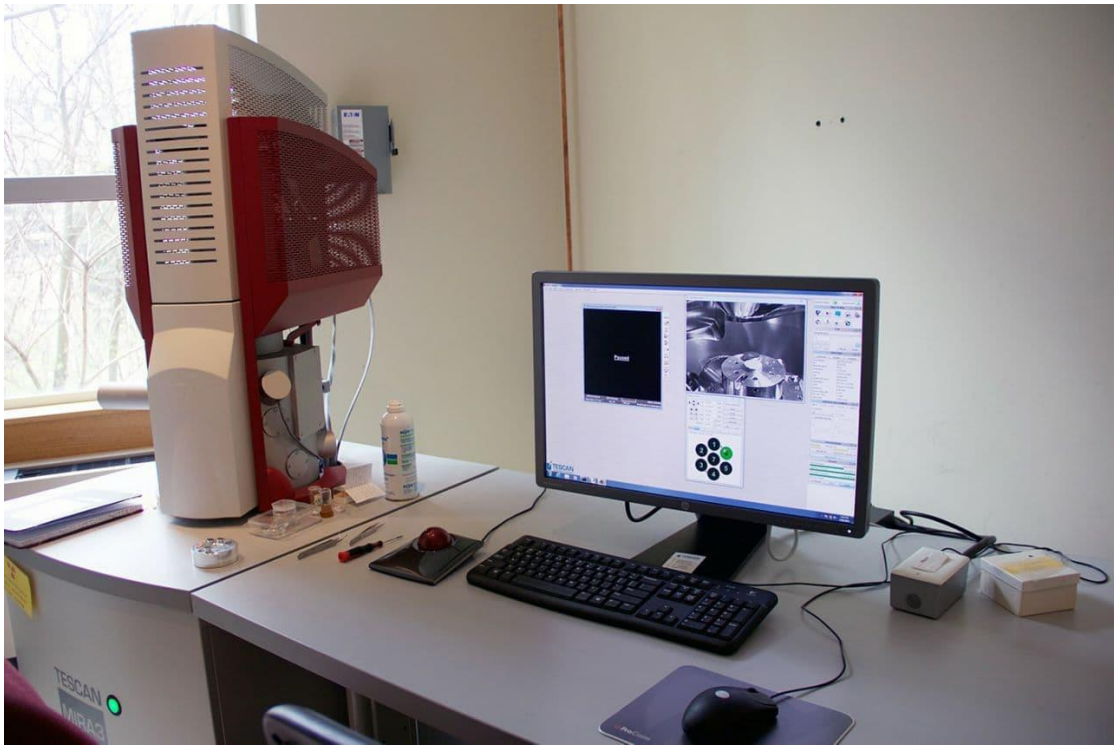

Fig.(3-4): Diagram for system of SEM device.

3.4.4 Optical Properties Measurements

The absorption spectra of (PMMA/Si_3N_4/TaC) nanocomposite films were recorded in the wavelength range (200-1100) nm using the double-beam spectrophotometer (Shimadzu, UV-1800 A0, Japan), as shown in figure (3-5) has been introduced at the University of Babylon / College of Education for Pure Science /Physics. The absorption spectrum being recorded at RT. To obtain the absorbance, transmittance, absorption coefficient, indirect transition, extinction coefficient, refractive index, dielectric constant (real and imaginary parts), a computer program (UV Probe software) was used.

Fig. (3-5) UV Photographic of spectrophotometer

3.4.5 Measurement of A.C. Electrical Conductivity

It was determined within the frequency range (100 Hz-5×10^6 Hz) at RT by measuring the capacitor and the loss angle tangent as a function of the alternating electric field frequency using the (LC.R meter). The Agilent impedance analyzer was measured within the above-mentioned frequency ranges using software in the apparatus. Figure (3-6) displays an A.C circuit diagram.

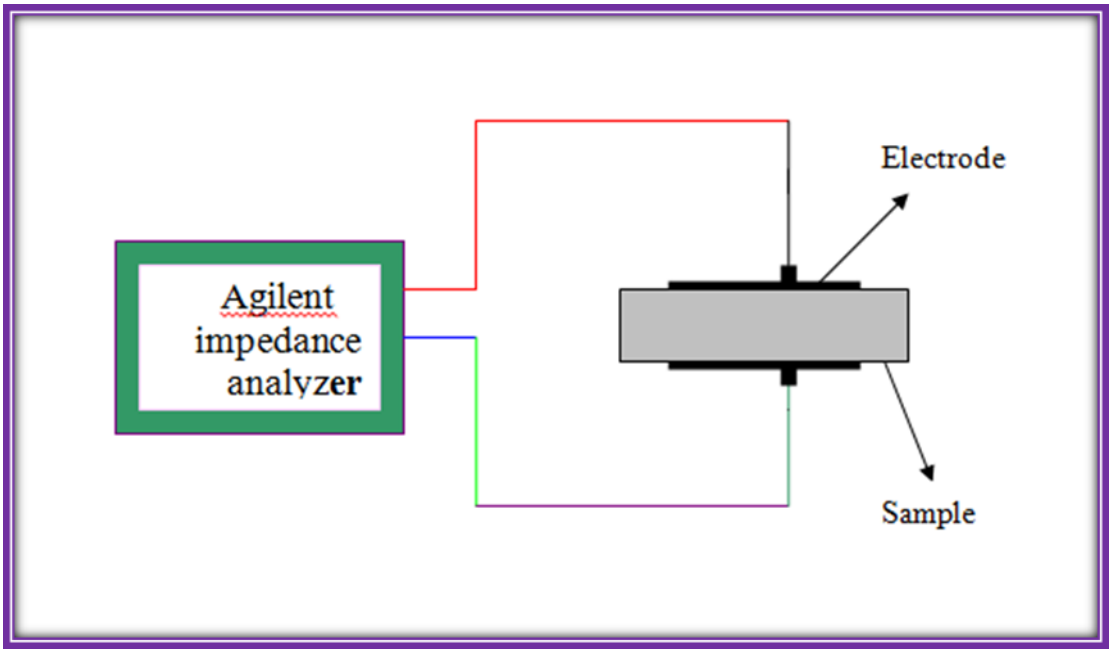

Fig. (3-6) Diagram for system of A.C electrical measurement

3.5 Antibacterial Activity Application Measurements of Nanocomposites

Antimicrobial activity of the (PMMA/Si_3N_4/TaC) nanocomposites tested samples were determined using a disc diffusion method. The antibacterial activities were done by using gram positive organisms (Staphylococcus aureus) and gram-negative organisms (Klebsiella aerogenes). Bacteria (Staphylococcus aureus and Klebsiella aerogenes) were cultured in Muller-Hinton agar. The films of the (PMMA/Si_3N_4/TaC) nanocomposites were placed over the media and incubated at 37 °C for 24 hours. The inhibition zone diameter was measured.

Chapter Four

Results, Discussion and Conclusions

4.1 Introduction

This chapter included the results and its discussion of the structural, optical and A.C electrical measurements for (PMMA/Si_3N_4/TaC) nanocomposites. It will also discuss the effect of different concentrations additive nanoparticles (Si_3N_4/TaC) in the optical microscope, Fourier transform infrared rays (FTIR), field emission scanning electron microscope (FE-SEM) and antibacterial activity applications of (PMMA/Si_3N_4/TaC) nanocomposites are also discussed.

4.2 The Structural Properties

4.2.1 The Optical Microscope

The optical microscope gives the change of surface morphology of (PMMA/Si_3N_4/TaC) nanocomposites. Figure (4-1) displays the (PMMA/Si_3N_4/TaC) nanocomposites optical microscope (OM) at magnification power (10x). Image(A) shows a uniform phase without phase separation; in the other hand, it has a finer morphology and smooth surface, demonstrating at this successful polymer ratio of PMMA. While image (B-E), it can be seen, that (Si_3N_4/TaC) NPs are well dispersed on the surface of the PMMA polymer films and this apparent more evident with the increase in the wt.% of (Si_3N_4/TaC). The nanocomposite shows nearly elliptical structure of particles of uniform shape. This is because the NPs have a large surface area while the polymeric solution containing different polar groups has a high affinity for (Si_3N_4/TaC) which leads to the orientation of the nanoparticles within the polymer chain and thus the (Si_3N_4/TaC) structure becomes more compact and thus the consistency of the material increases. This provided a suitable preparation method for preparing nanocomposite films [103,104].

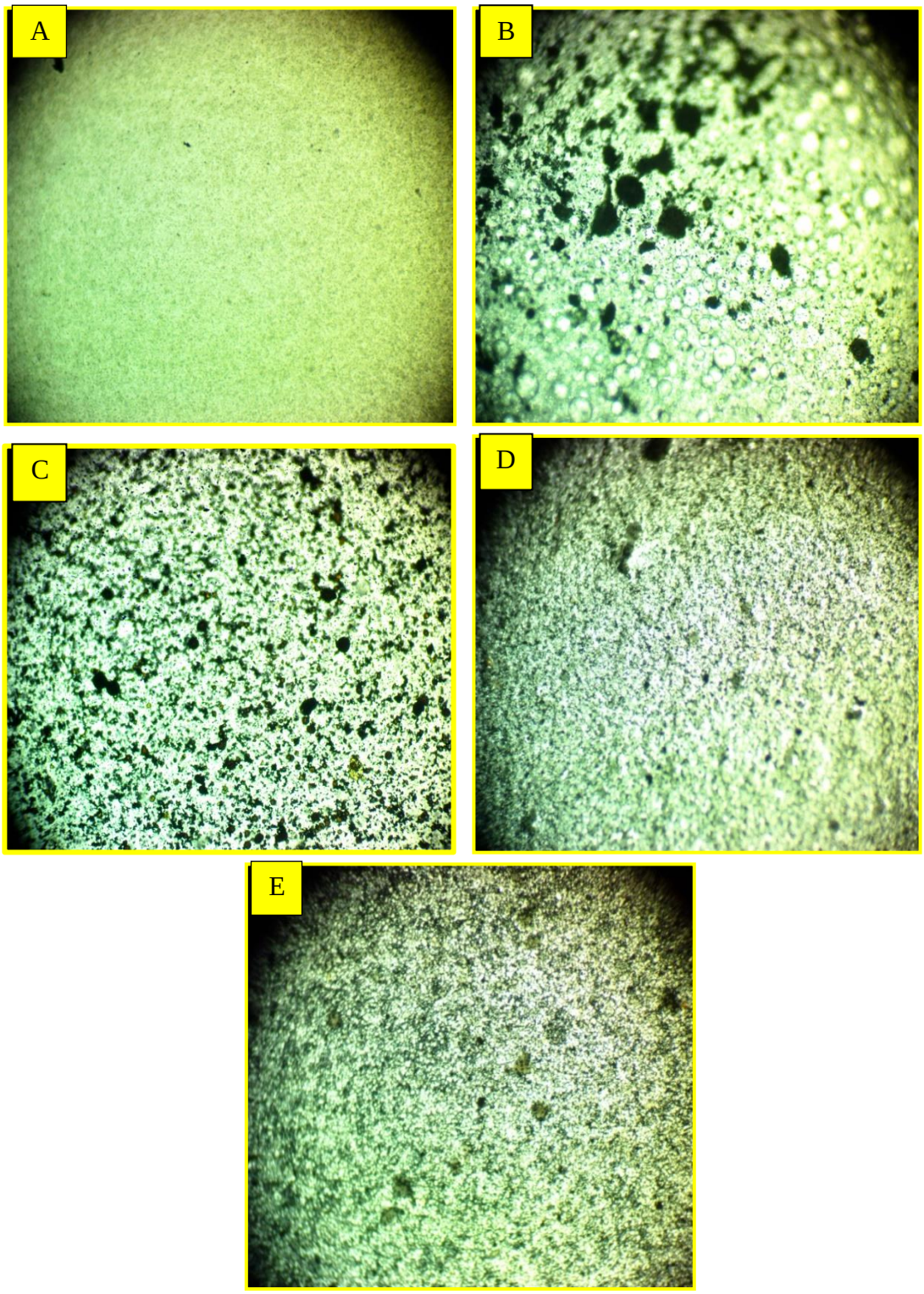

Fig. (4-1) Images of OM (10x) for (PMMA/Si_3N_4/TaC) nanocomposites A. pure polymer, B. 2 wt.% of (Si_3N_4/TaC) NPs, C. 4 wt.% of (Si_3N_4/TaC) NPs, D. 6 wt.% of (Si_3N_4/TaC) NPs and E. 8 wt.% of (Si_3N_4/TaC) NPs.

4.2.2 Fourier Transform Infrared Rays (FTIR)

FTIR spectra provide information on the vibration and rotation of molecular groups in a material. Figure (4-2) displays the FTIR spectra of (PMMA/Si_3N_4/TaC) nanocomposites in the wave number range (500–4000) cm^{-1}. In image (A), FTIR spectra of (PMMA) polymer are reveals absorption band at 2950.45 cm^{-1} corresponding to the CH_3 bending vibration and the band 1723.22 cm^{-1} attributed to the C=O stretching vibration. CH_3 stretching vibration indicate to the band 1434.60 cm^{-1}. The absorption band at 1142.95 attribute to the symmetric stretching vibration of C-O. The bands 985.57 cm^{-1}, 698.13 cm^{-1} and 750.29 cm^{-1} corresponding to the C−C bending and stretching vibration respectively [105].

The spectra of PMMA with variant concentration of Si_3N_4 / TaC NPs in images B, C, D, and E respectively. In image B where the additive 2 wt.% (Si_3N_4 / TaC) NPs caused shift in some bands and intensities at low wavenumber (1434.63, 1142.83) cm^{-1} and high wave number at bands (1723.30, 995.01, 750.01) cm^{-1}but bands 2950.45 cm^{-1} and 698.13 cm^{1} there is not affected on this band, while the image C the additive concentration of 4 wt.% of Si_3N_4/TaC NPs, affected change shift in some bands and intensities at low wavenumber (995.34, 750.45) cm^{-1} and high wave number at bands (1723.45, 1434, 1143) cm^{-1} while the 2950.45 cm^{-1} and 698.13 cm^{1} there is not affected on this band. the image D which additive concentration of 6 wt.% of Si_3N_4/TaC NPs, shifted and changed several bands' intensity at low wavenumber (995.42, 750.02) cm^{-1} and high wave number at bands (1723.54, 1434.64, 1143) cm^{-1}but bands 2950.45 cm^{-1} and 698.13 cm^{1} has not been impacted and added concentration of 8 wt.% from(Si_3N_4/TaC) NPs in image E, caused shifts in certain bands and intensities at low wavenumber (994.90, 749.93) cm^{-1} and high wave number at bands (1724.04, 1434.68, 1143) cm^{-1}but bands

2950.45 cm^{-1} and 698.13 cm^{1} has not been impacted. The FTIR studies show that adding different concentration of (Si_3N_4/TaC) in images B, C,D and E leads to the displacement of some of the bonds and not emergence of new peaks therefore, there is no interaction between (Si_3N_4/TaC) nanoparticle and the PMMA polymer matrix. The spectra characteristic bands of stretching and bending vibrations of the functional groups formed in nanocomposites were displayed in Tables (4.1).

Table (4.1): FTIR-characteristic for (PMMA/Si_3N_4/TaC) Nanocomposites

band	0wt% Si_3N_4/TaC	2wt% Si_3N_4/TaC	4wt% Si_3N_4/TaC	6wt% Si_3N_4/TaC	8wt% Si_3N_4/TaC
(CH_3) bending Vibration	2950.45	2950.45	2950.45	2950.45	2950.45
(C-O) Stretching Aldehyde (1720-1740) cm^{-1}	1723.22	1723.30	1723.45	1723.54	1724.04
(C=O) Stretching vibration	1434.60	1434.63	1434	1434.64	1434.68
(CH_3) Stretching vibration	1142.95	1142.83	1143	1143	1143
(C-O) Symmetric stretching vibration	985.57	995.01	995.34	995.42	994.90
(C-C) bending vibration	750.29	750.01	750.45	750.02	749.93
aromatic ring out of plane bends	698.13	698.13	698.13	698.13	698.13

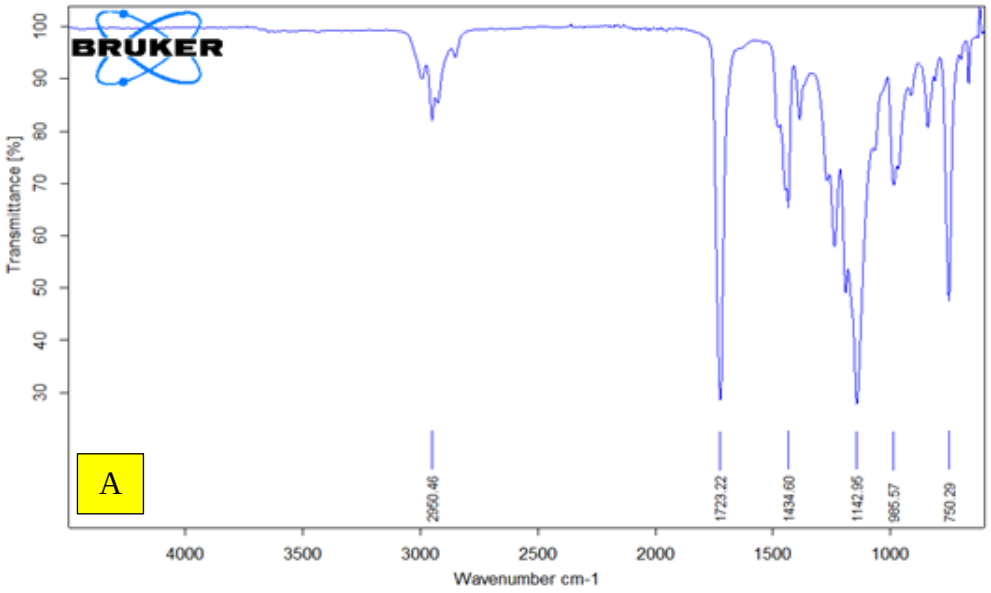
BRUKER
Transmittance [%]
100
90
80
70
60
50
40
30
A
2950.46
1723.22
1434.60
1142.95
985.57
750.29
4000
3500
3000
2500
2000
1500
1000
Wavenumber cm-1

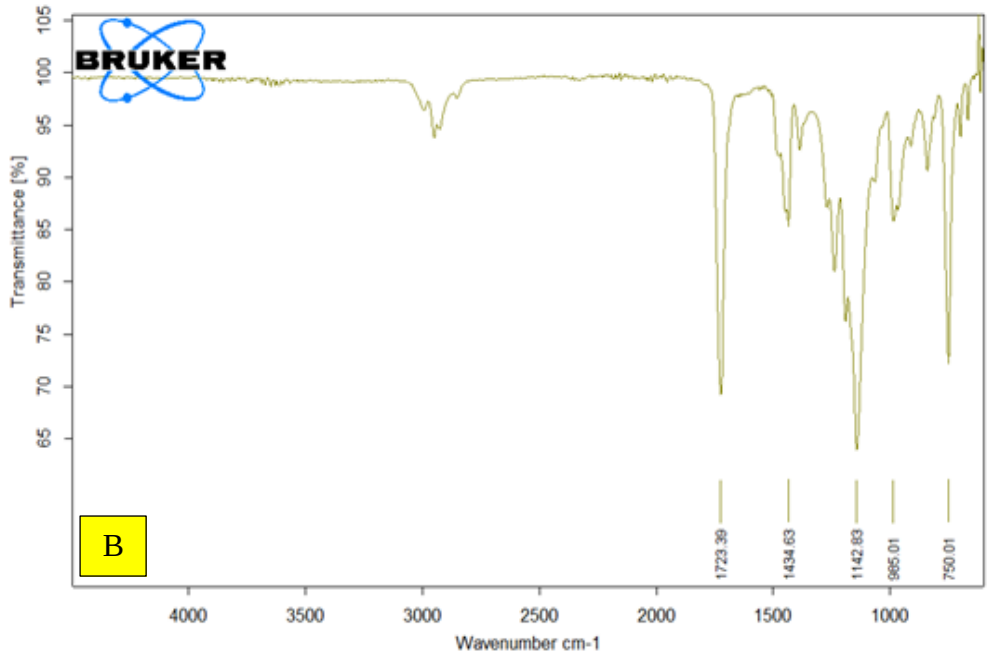
BRUKER
Transmittance [%]
105
100
95
90
85
80
75
70
65
B
1723.39
1434.63
1142.83
985.01
750.01
4000
3500
3000
2500
2000
1500
1000
Wavenumber cm-1

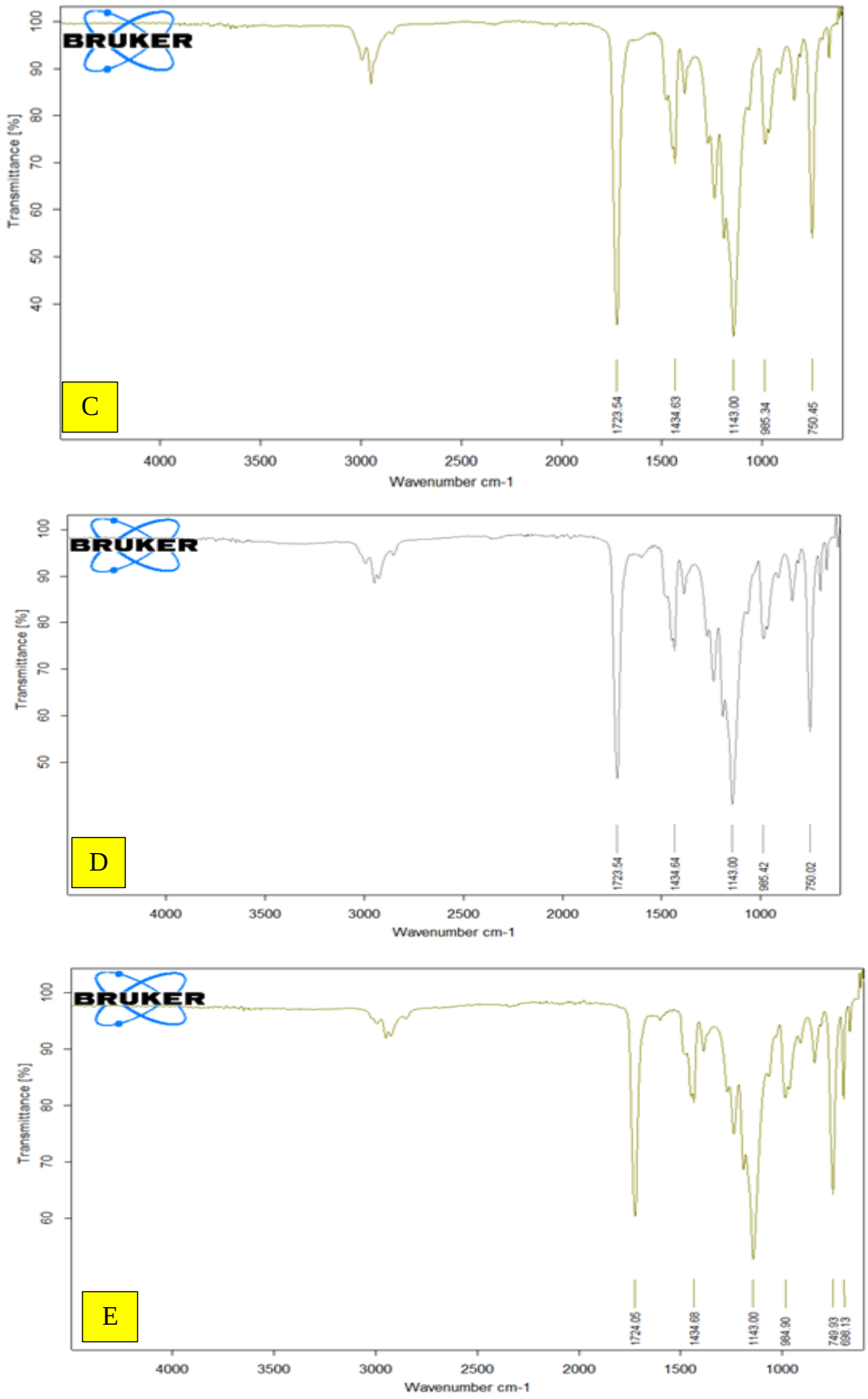

Fig.(4-2) FTIR spectra of (PMMA/Si_3N_4/TaC) nanocomposites A. pure polymer, B. 2 wt.% of (Si_3N_4/TaC) NPs, C. 4 wt.% of (Si_3N_4/TaC) NPs, D. 6 wt.% of (Si_3N_4/TaC) NPs and E. 8 wt.% of (Si_3N_4/TaC) NPs.

4.2.3 Field Emission Scanning Electron Microscopy (FE-SEM)

To examine the morphological of (PMMA/Si_3N_4/TaC) nanocomposites using field emission scanning electron microscopy (FE-FE-SEM). Figure (4-3) demonstrates the FE-SEM images of pure PMMA and (PMMA/Si_3N_4/TaC) nanocomposites with various concentration (2, 4, 6 and 8 wt.%) of Si_3N_4/TaC NPs with a magnification power 20 KX and scale 200 nm. The homogenous and uniform distribution of pure PMMA in this figure in image A which mean a successful this method to prepare film. The regular distributed of Si_3N_4 /TaC NPs inside the PMMA matrix that explained in images (B, C, D and E) respectively, which attributed to strong covalent interaction between the (Si_3N_4 / TaC) NPs in the PMMA matrix [19]. It is clear from histogram in figure (4-4) which obtain the distribution of grain size (Si_3N_4 / TaC) NPs inside the PMMA polymer matrix. From this histogram, it can be obtain that the grain size decreased with increasing concentration of (Si_3N_4 / TaC) NPs, which decreased from 136.76 nm for pure PMMA to 61.84 nm for 8% wt. of Si_3N_4/TaC NPs concentration, which indicate a good homogenous distribution concentration of(Si_3N_4 / TaC) NPs inside the PMMA polymer matrix without aggregation or clusters.

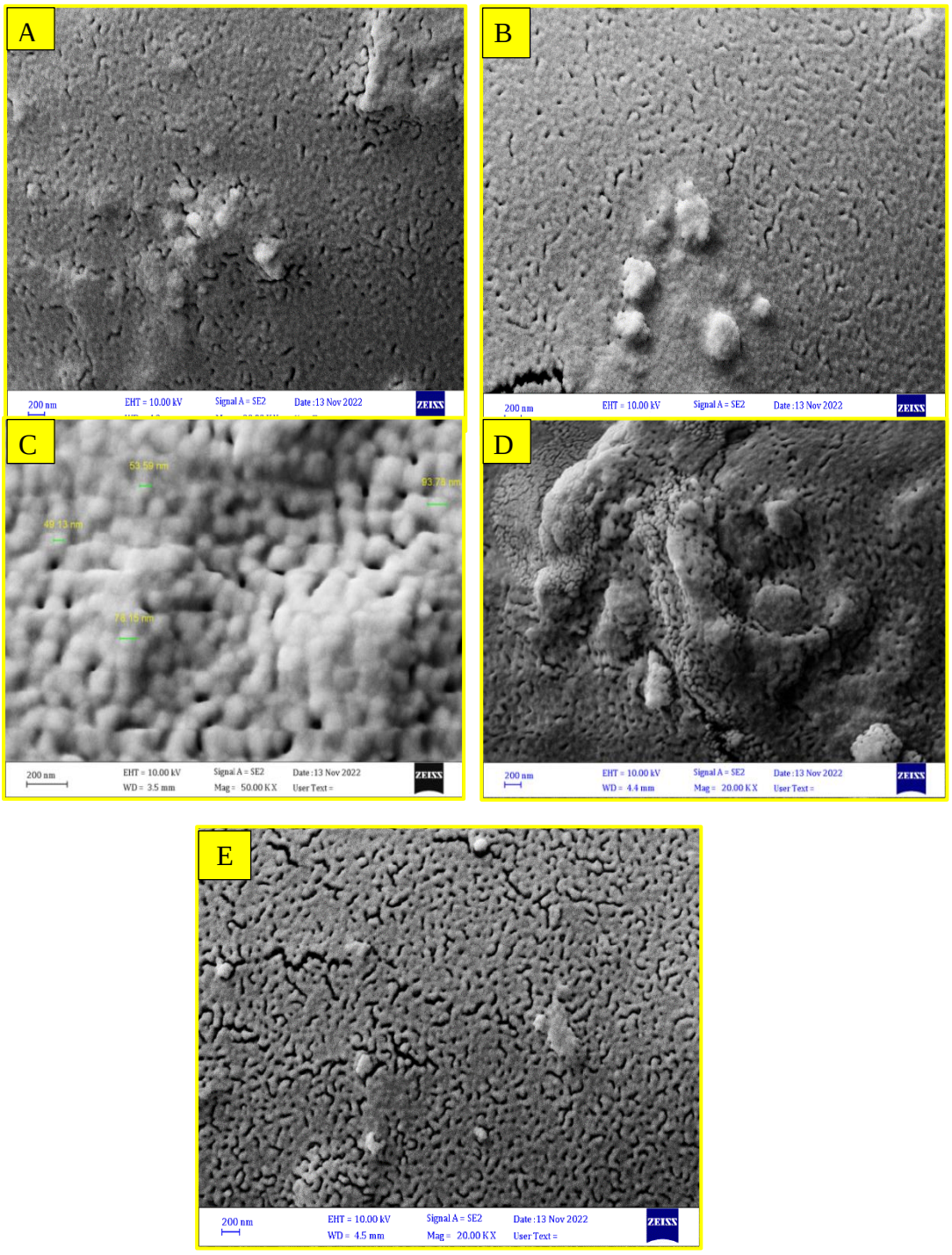

Fig. (4-3) FE-SEM images of (PMMA/Si_3N_4/TaC) nanocomposites, (A) for (PMMA), (B) 2 wt.% Si_3N_4 / TaC NPs, (C) 4 wt.% Si_3N_4 / TaC NPs, (D) 6 wt.% Si_3N_4 / TaC NPs, (E) 8 wt.% Si_3N_4 / TaC NPs

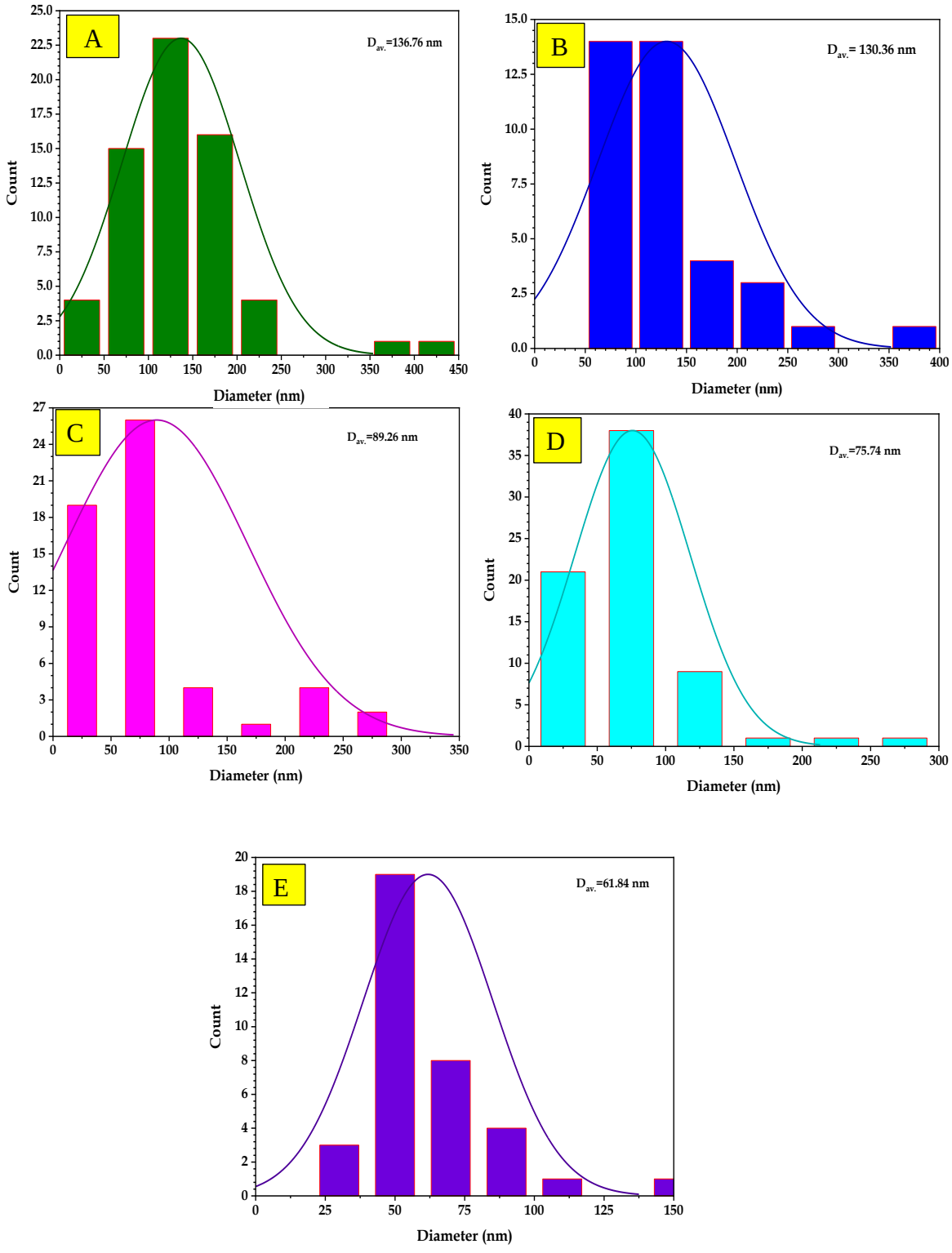

Fig. (4-4) Histogram of (PMMA/Si_3N_4/TaC) nanocomposites, (A) for (PMMA), (B) 2 wt.%(Si_3N_4 / TaC) NPs, (C) 4 wt.%(Si_3N_4 / TaC) NPs, (D) 6 wt.%(Si_3N_4 / TaC) NPs, (E) 8 wt.%(Si_3N_4 / TaC) NPs

4.3 Optical Properties

The main purpose of studying the optical properties of the PMMA/Si_3N_4/TaC nanocomposites is to identify the effect of adding Si_3N_4/TaC nanoparticles on the optical properties of (PMMA) films. The research covers the recording of the spectrum of absorbance for the (PMMA/Si_3N_4/TaC) films at room temperature and calculating the absorption coefficient, extinction coefficient, and other optical constants, as well as identifying the types of electronic transitions and calculating energy gaps.

4.3.1 The Absorbance

The absorption of PMMA/Si_3N_4/TaC nanocomposite with various content of Si_3N_4/TaC NPs were recorded at wavelengths range 200-1100 nm at room temperature. The absorbance for PMMA/Si_3N_4/TaC nanocomposites with wavelength is demonstrate in figure (4-5). From this figure, the absorption increases with increasing content of Si_3N_4/TaC NPs. This is due to donor level electrons being excited to the conduction band at high energies. Also, because photons provide enough energy to react with atoms, an electron can be excited from a lower to a higher energy level by absorption an established photon [106-108].

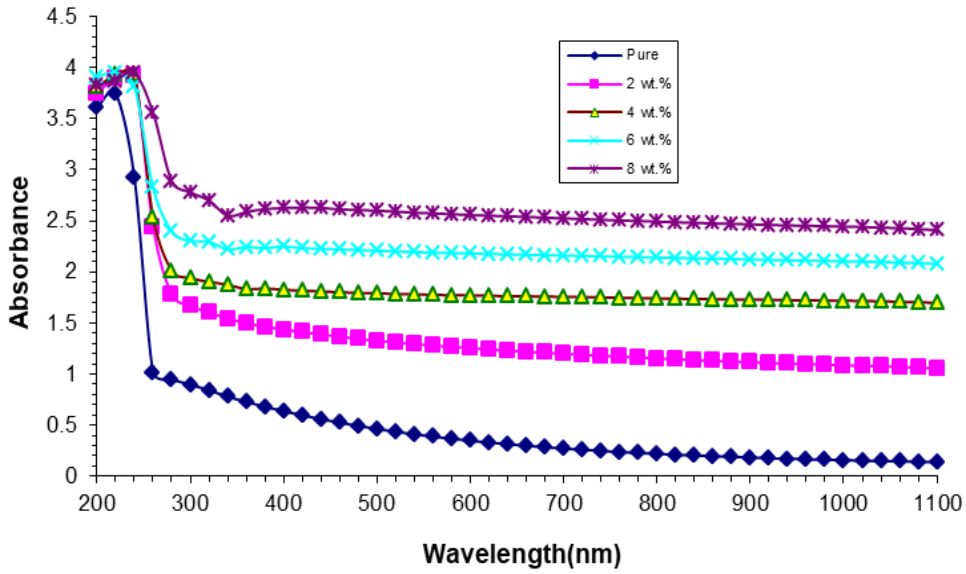

Fig.(4-5) The absorbance of (PMMA/Si_3N_4/TaC) nanocomposites with wavelength.

4.3.2 Transmittance Spectrum

The transmittance of (PMMA/Si_3N_4/TaC) nanocomposite was calculated from equation (2-13). Figure (4-6) demonstrate the transmittance of (PMMA/Si_3N_4/TaC) nanocomposite with wavelength. The transmittance reduces as the number of(Si_3N_4/TaC) nanoparticles increase, which is due to the agglomeration of nanoparticles with increasing content [109].

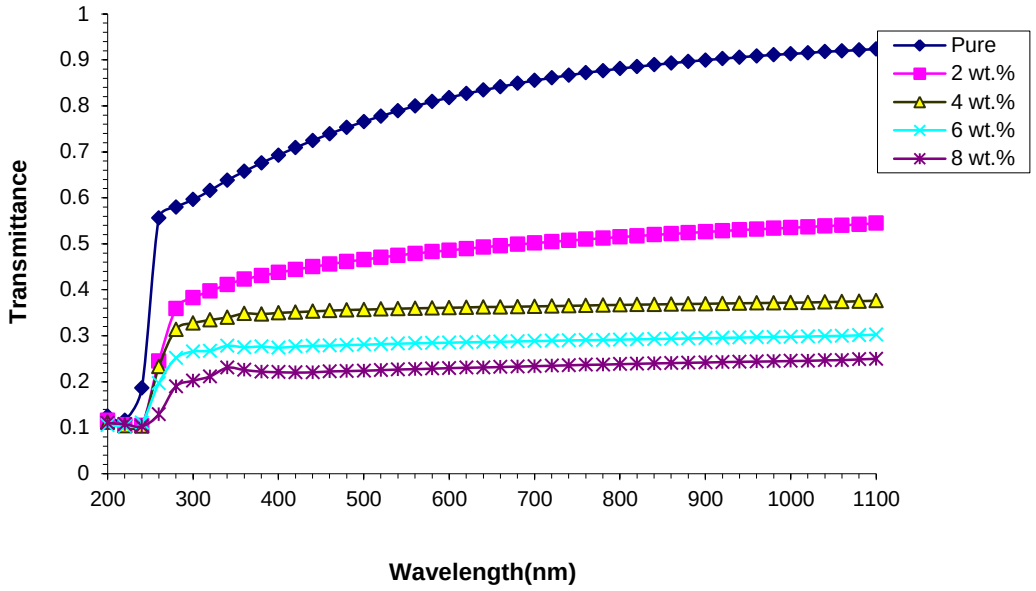

Fig. (4-6) Variation transmittance of (PMMA/Si_3N_4/TaC) nanocomposites with wavelength.

4.3.3 Absorption Coefficient

The absorption coefficient of nanocomposites was calculated by equation (2-11). Figure (4-7) explain the absorption coefficient of (PMMA/Si_3N_4/TaC) nanocomposite versus photon energy of the incident light. The absorption coefficient gives information of kind of electron transition. It is assumed that direct electron transitions occur when the material's absorption coefficient is large (>10^4) cm^{-1}. When the material's coefficient of absorption is low 10^4 cm^{-1}, an indirect transition of electrons is assumed. The values of absorption coefficient of (PMMA/Si_3N_4/TaC) nanocomposite, the transition of electron is indirect. The coefficient of absorption of nanocomposites increase with the increasing of the content of Si_3N_4/TaC nanoparticles, this is due to the rise of number of charge carriers and therefore rising the absorbance and absorption coefficient for (PMMA/Si_3N_4/TaC) nanocomposites[110-112].

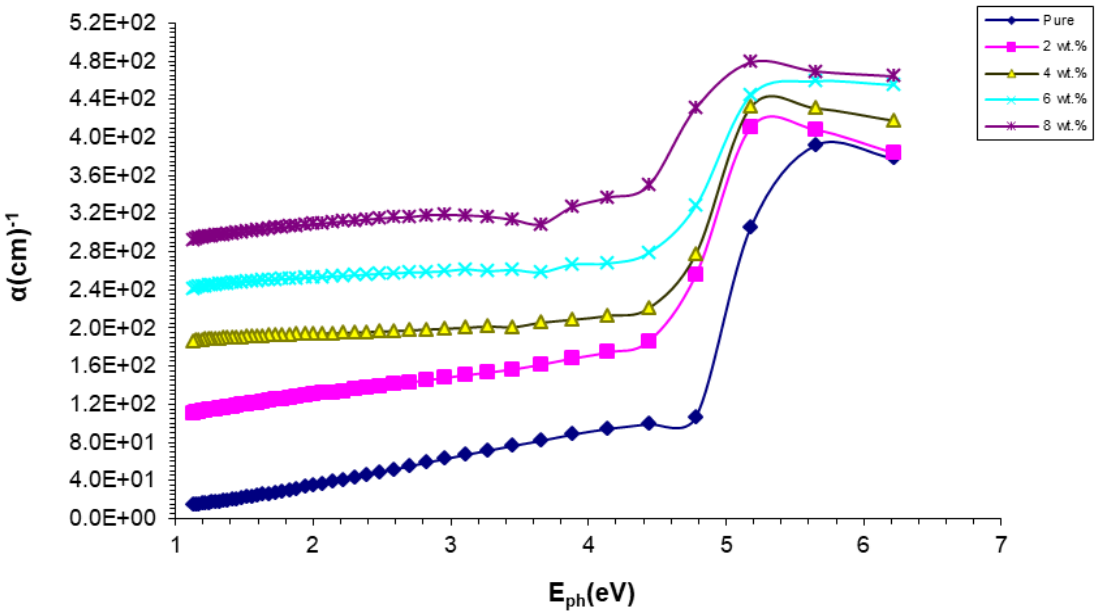

Fig. (4-7) The coefficient of absorption of (PMMA/Si_3N_4/TaC) nanocomposites with photon energies.

4.3.4 Optical Energy Gaps of the Indirect Transition (Allowed and Forbidden)

The energy band gap of (PMMA/Si_3N_4/TaC) nanocomposites were calculated by equation (2-7). The energy gap for allowed and forbidden indirect transitions of (PMMA/Si_3N_4/TaC) nanocomposites are explain in figures (4-8) and (4-9) respectively. We may find the energy gap for the indirect transition by plotting the data or tang cut from the top of the curve to the (x- axis) at $((\alpha h\upsilon)^{1/2}=0$) [113]. From these figures, the energy gap for allowed and forbidden indirect transitions are reduce with the rises of the Si_3N_4/TaC nanoparticles content, this action is due to the formation of levels in the energy gap and therefore these local levels reduce the energy gap with rise of the Si_3N_4/TaC nanoparticles content. The value of the energy gap of nanocomposites are listed in Table (4-1). This result is agreed with researchers [114].

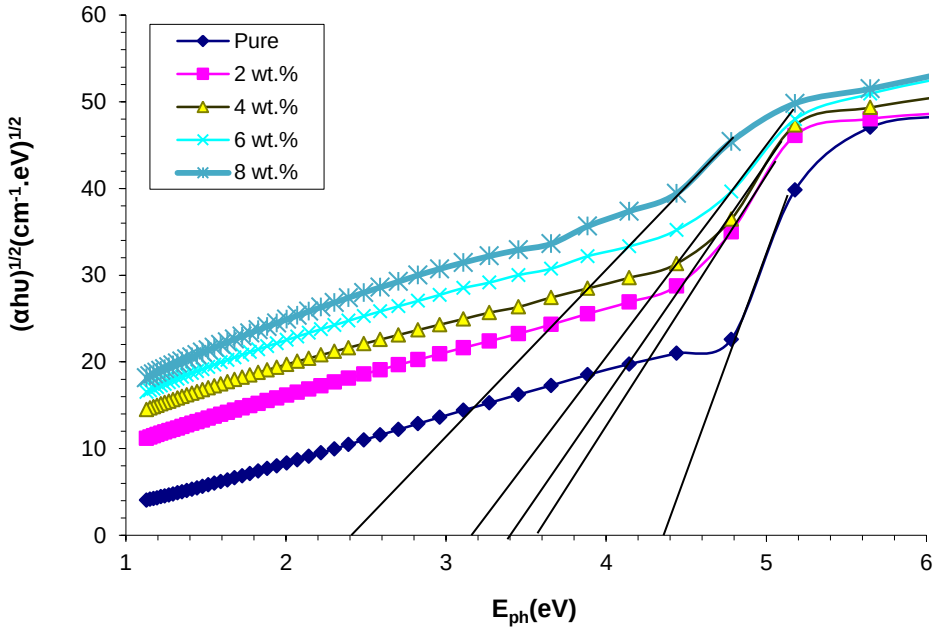

Fig. (4-8) The gap of energy for the allowed indirect transition $(\alpha h\nu)^{1/2}$ $(cm^{-1}.eV)^{1/2}$ of (PMMA/Si_3N_4/TaC) nanocomposites

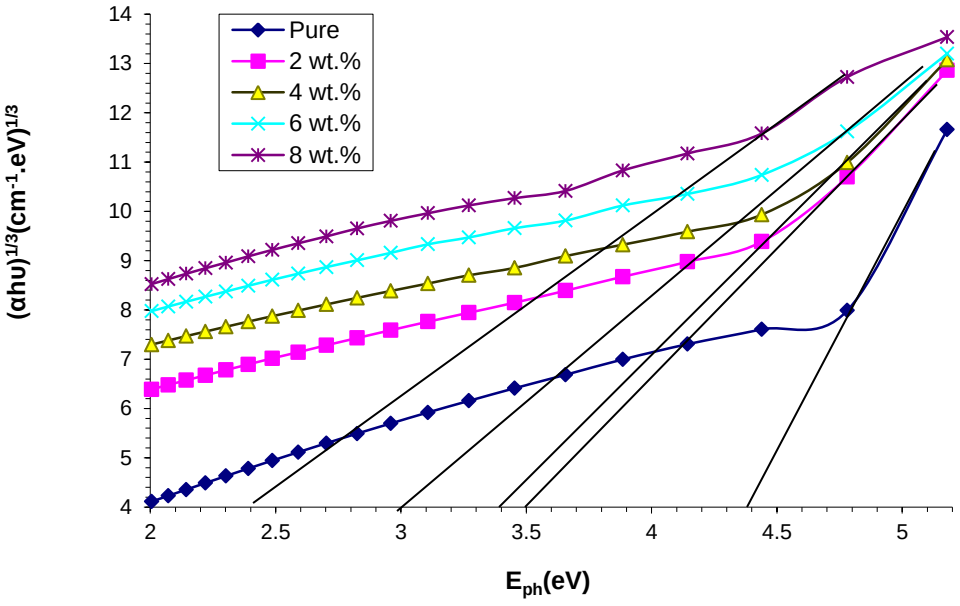

Fig. (4-9) The energy gap for the forbidden indirect transition $(\alpha h\nu)^{1/3}$$(cm^{-1}.eV)^{1/3}$ of (PMMA/Si_3N_4/TaC) nanocomposites

Table (4-2) The values gap of energy of (PMMA/Si_3N_4/TaC) nanocomposites

Si_3N_4/TaC NPs wt% content	Allowed of indirect energy gap (eV)	Forbidden of indirect energy gap (eV)
0	**4.4**	**4.4**
2	**3.6**	**3.5**
4	**3.4**	**3.4**
6	**3.2**	**3.0**
8	**2.4**	**2.4**

4.3.5 Refractive Index

The refractive index (n) is calculated by using equation (2-9). The refractive index of (PMMA/Si_3N_4/TaC) nanocomposites versus wavelength are shown in figure (4-10). It is obtained that the refractive index increases with the increasing of the content of Si_3N_4/TaC NPs. This action due to the increase of the density of nanocomposites [115,116].

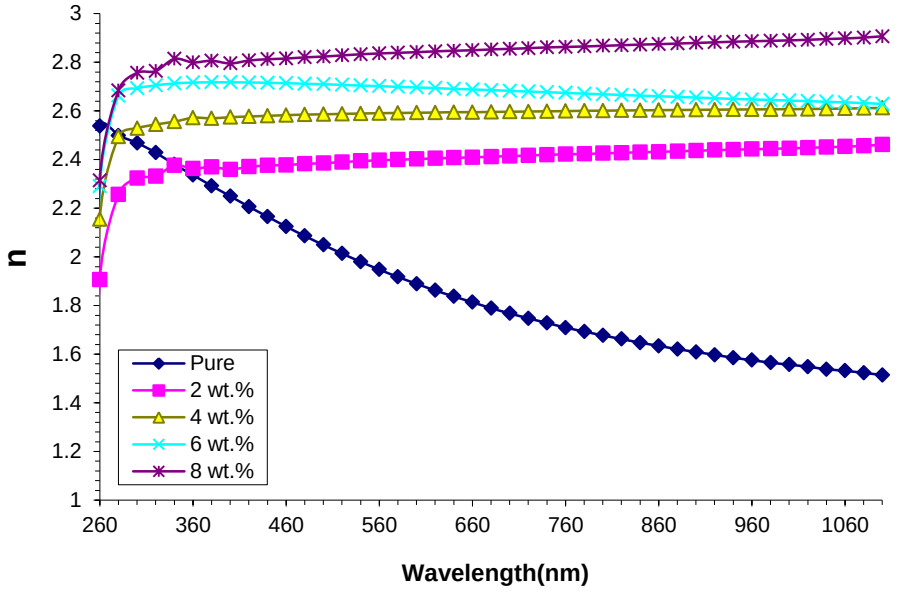

Fig. (4-10) The refractive index for (PMMA/Si_3N_4/TaC) nanocomposites with wavelength

4.3.6 Extinction Coefficient

The extinction coefficient (k) was calculated by using the equation (2-10). Figure (4-11) demonstrates the extinction coefficient of (PMMA/Si_3N_4/TaC) nanocomposites versus of wavelength. It is observed that the extinction coefficient of nanocomposites increases with the increasing of the Si_3N_4/TaC content, which attributed to the rise in absorbance and photons distribution in the PMMA polymer matrix [117].

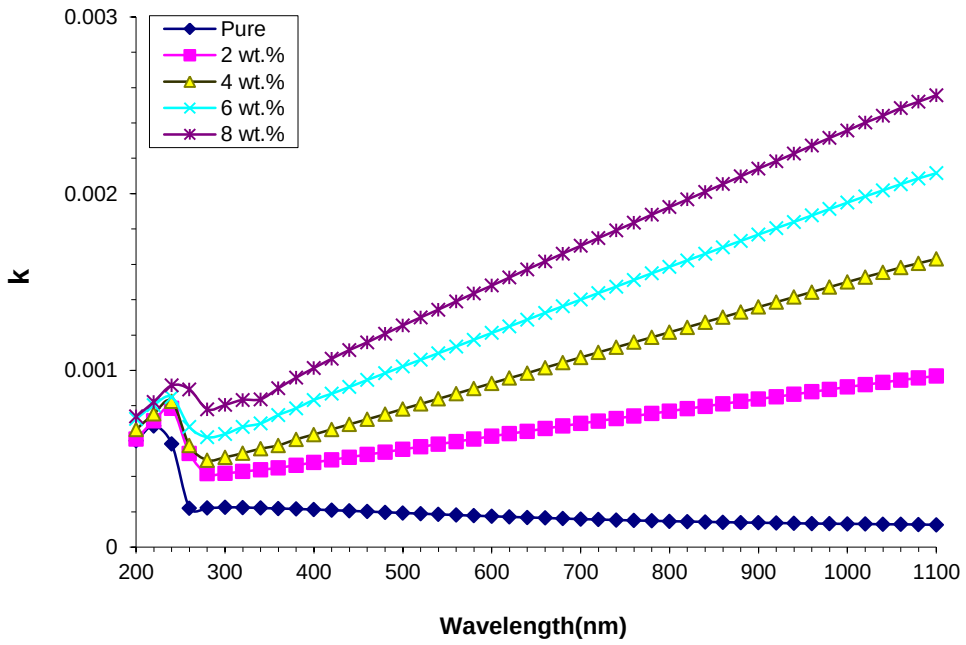

Fig. (4-11) The coefficient of extinction for (PMMA/Si_3N_4/TaC) nanocomposites with wavelength.

4.3.7 Real and Imaginary Parts of Dielectric Constant

By using the equations (2-15) and (2-16) to calculated the real and imaginary parts of dielectric constant. The real (ε_1) and imaginary (ε_2) parts of dielectric constant for (PMMA/Si_3N_4/TaC) nanocomposites with wavelength are explain in figures (4-12) and (4-13). From the figures, the real and imaginary parts of dielectric constant of nanocomposite are increase with the increasing of (Si_3N_4/TaC) NPs content and reduce with

rising wavelength, this result was caused by the sample's nanoparticles content, which led to an increase in electrical polarization [118]. This is because extinction coefficient affects the real components of the dielectric constant independently of refractive index, whereas extinction coefficient affects the imaginary components of the dielectric constant [119].

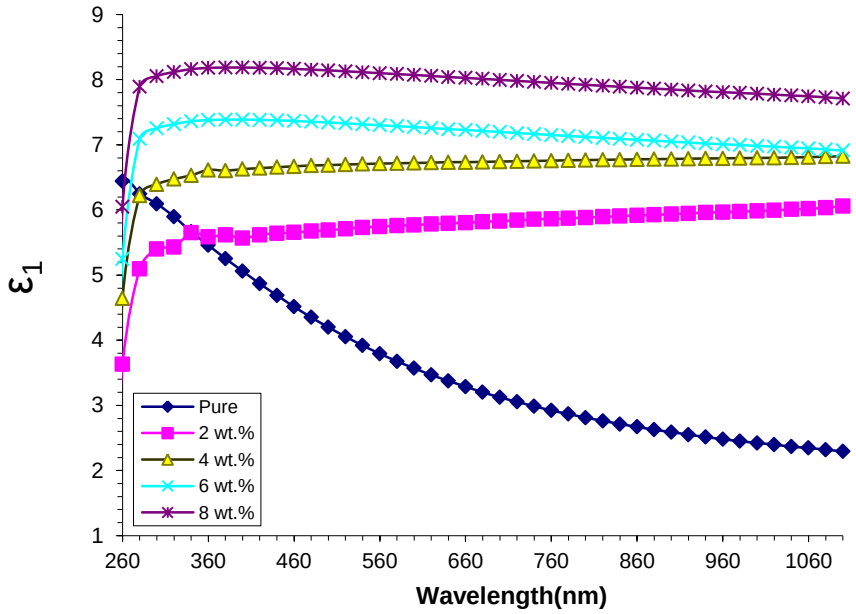

Fig. (4-12) Dielectric constant of real part of (PMMA/Si_3N_4/TaC) nanocomposites with wavelength.

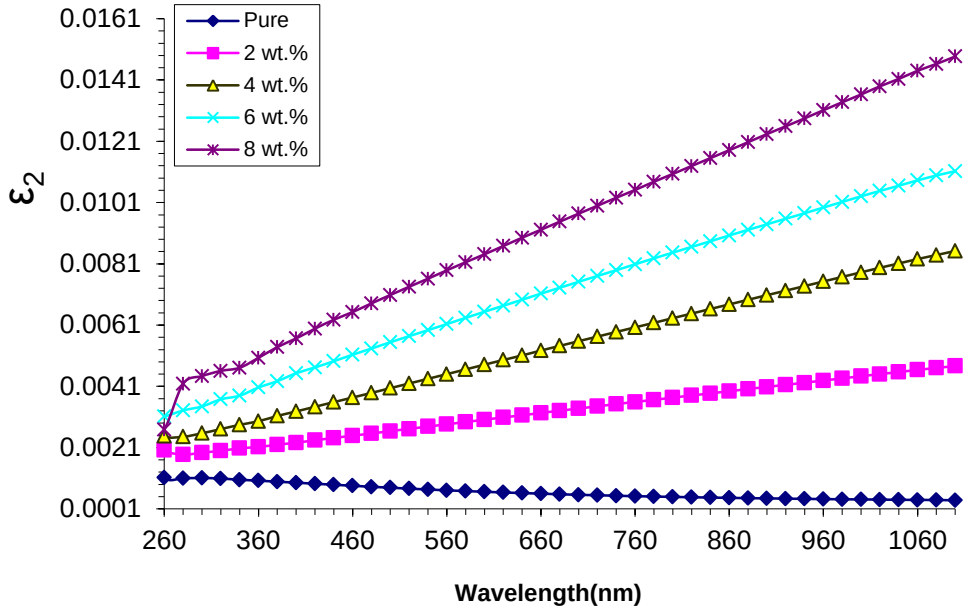

Fig. (4-13) Variation imaginary parts of dielectric constant of (PMMA/Si_3N_4/TaC) nanocomposites with wavelength.

4.3.8 Optical Conductivity

The optical conductivity ($\sigma_{opt.}$) was calculated from the equation (2-17). The σ_{op} of (PMMA/Si_3N_4/TaC) nanocomposites with a wavelength are explain in figure (4-14). According to this figure, the localized phases of density in the structure of band increases with increasing nanoparticle content, which is due to the formation of levels of localized in the gap of energy. As a result, increase in the absorption coefficient implies an increase in the optical conductivity of the nanocomposite [120].

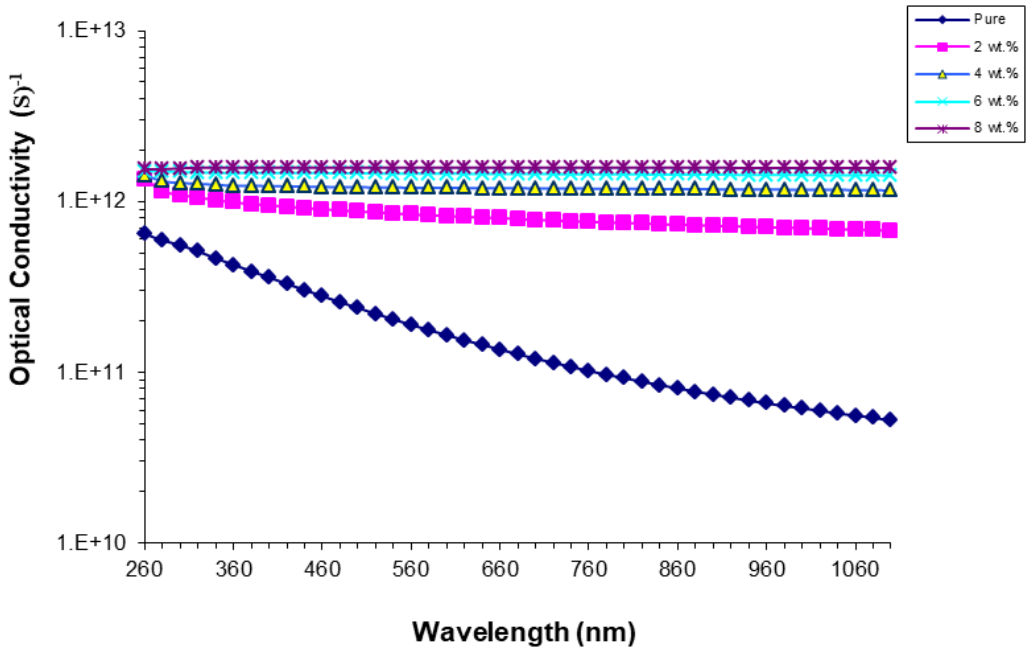

Fig. (4-14) Variation of optical conductivity of (PMMA/Si_3N_4/TaC) nanocomposites with wavelength.

4.4 The A.C Electrical Properties of (PMMA/Si_3N_4/TaC) nanocomposites

The (PMMA/Si_3N_4/TaC) nanocomposites were investigated for their alternating current (A.C) electrical properties between 100Hz and 5MHz at room temperature. In order to identify the dielectric constant, that is the most essential of A.C characteristic, we used the equation (2-40). The dielectric loss can be calculated by the dielectric constant and (tan δ), using the equation (2-34), while A.C electrical conductivity (σ_{AC}) can be calculated by equation (2-41) by substituting the values of (ε'').

4.4.1 The dielectric constant for (PMMA/Si_3N_4/TaC) nanocomposites

Figure (4-15) explain the dielectric constant of (PMMA/Si_3N_4/TaC) nanocomposites with frequency. It is note that dielectric constant decrease with rising of frequency for all the sample prepare which, as a result of the capabilities of dipoles in nanocomposites samples to transform in the direction of the applying electric current and the

reduction of space charge polarization [121]. Figure (4-16) explain the dielectric constant of (PMMA/Si_3N_4/TaC) nanocomposite with the content of nanoparticle at 100Hz. It is observed that dielectric constant increase with increasing of concentration nanoparticle for all illustrations of nano-composites. Interfacial polarization in the nanocomposites' internal alternating electric field and an increase in the charge carriers are responsible for these processes of (PMMA/Si_3N_4/TaC) nanocomposite [122].

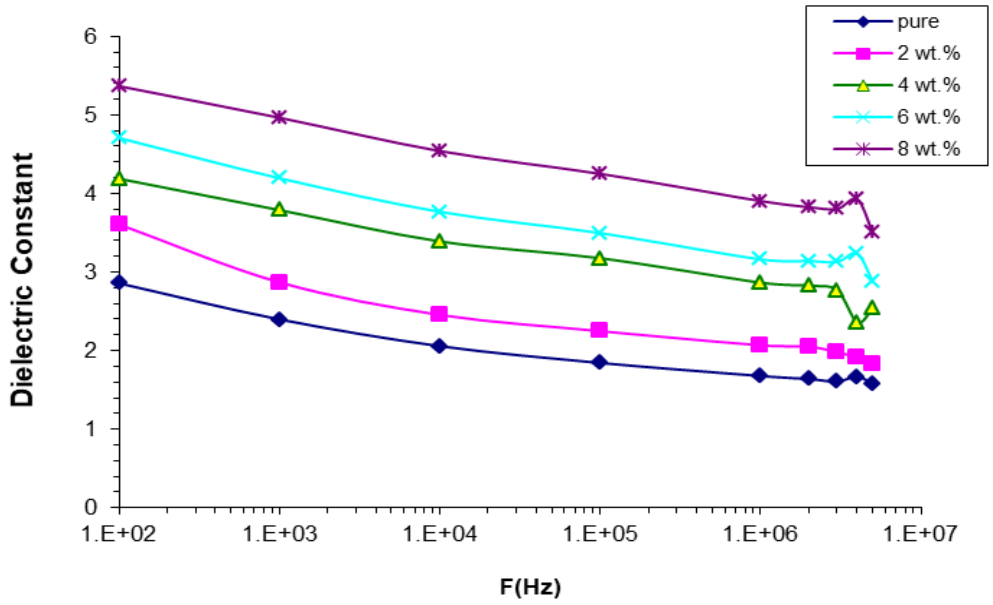

Fig. (4-15) Variation of dielectric constant with frequency of (PMMA/Si_3N_4/TaC) nanocomposite.

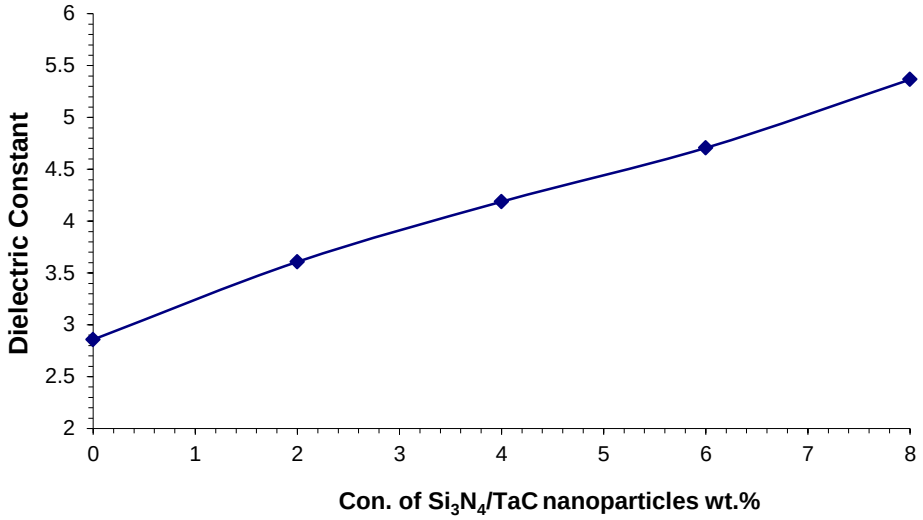

Fig. (4-16) Effect of (Si_3N_4/TaC) nanoparticles concentrations on dielectric constant for (PMMA/ Si_3N_4/TaC) nanocomposite at 100Hz.

4.4.2 The Dielectric Loss of (PMMA/Si_3N_4/TaC) Nanocomposites

Figure (4-17) shows the relationship between dielectric loss of (PMMA/Si_3N_4/TaC) nanocomposites and frequency. The dielectric losses for nanocomposites reduce as the frequency increases for all samples. This phenomenon was linked to a reduction in the contributions of polarization of space charges. According to the data, nanocomposites have a substantial dielectric loss at low frequencies. Due to the reduced time available for the dipoles to align at high frequencies, the dielectric loss decreases [123]. The dielectric loss of (PMMA/Si_3N_4/TaC) nanocomposites as a function of (Si_3N_4/TaC) NPs are shown in figure (4-18). From this figure, it is note that the dielectric loss increases with increasing content of the (Si_3N_4/TaC) nanoparticle. This result attributed to increased charge on the dipole [124].

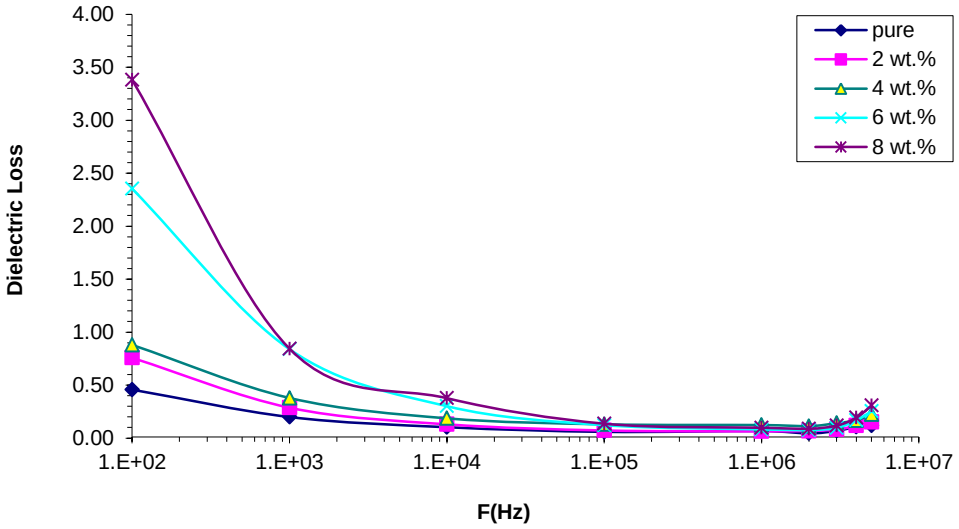

Fig. (4-17) Variation of dielectric loss with frequency of (PMMA/Si_3N_4/TaC) nanocomposite.

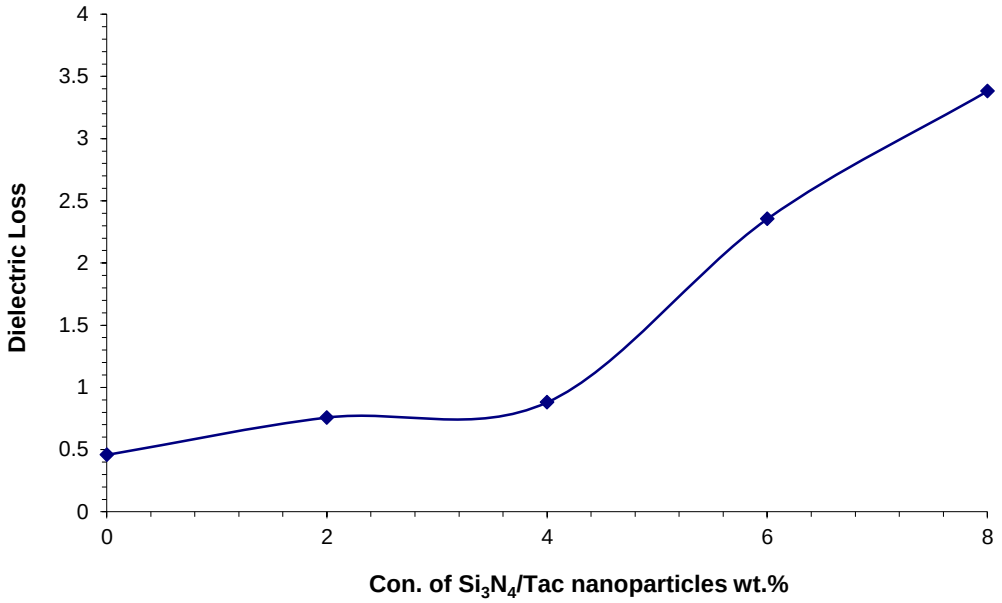

Fig.(4-18) Influence of(Si_3N_4/TaC) NPs concentrations on dielectric loss for (PMMA/ Si_3N_4/TaC) nanocomposite at 100Hz

4.4.3 The A.C Electrical Conductivity of (PMMA/Si_3N_4/TaC) Nanocomposites

Figure (4-19) shows the relationship between A.C electrical conductivity of (PMMA/Si_3N_4/TaC) nanocomposites and frequency. The mobility of charge carriers and the hopping of ions from the cluster cause the A.C electrical conductivity of all specimens to increase as the frequency of the electric field increases. At low frequencies, the number of mobile ions and electrical conductivity decreased due to increased charge accumulation at the electrode and electrolyte interface [125]. Because charge carriers moved more easily at high frequencies, the electrical conductivity of (PMMA/Si_3N_4/TaC) nanocomposites increase with frequency [126]. Figure (4-20) reveal that the electrical conductivity of nanocomposites increases with increasing of (Si_3N_4/TaC) nanoparticle content which due to increase in the ionic charge carriers and the formation of a continuous network of (Si_3N_4/TaC) nanoparticles inside polymer matrix [127,128]. The results of the ε', ε″, and A.C conductivity are shown in Table (4-2).

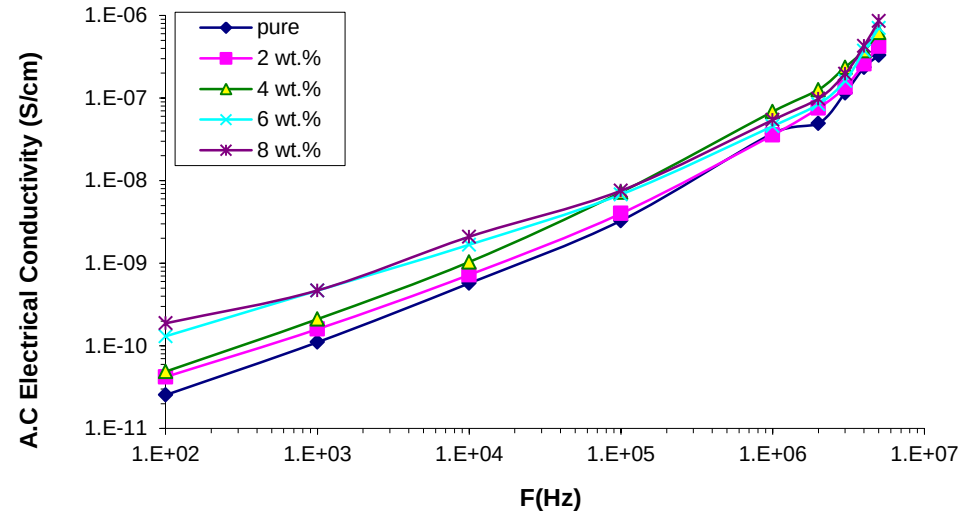

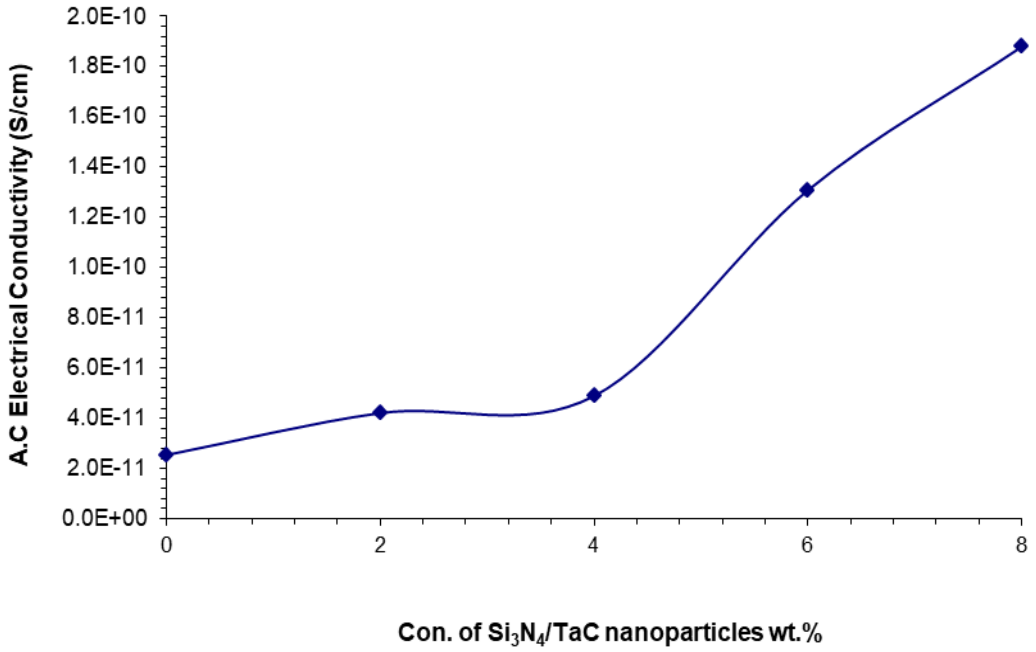

Fig. (4-20) Effect of (Si_3N_4/TaC) NPs content on AC electrical conductivity for (PMMA/Si_3N_4/TaC) nanocomposite at 100Hz.

Table (4-3) The values of dielectric constant, dielectric loss and AC electrical conductivity at 100 Hz of (PMMA/Si_3N_4/TaC) Nanocomposites.

Concentration of Si_3N_4/TaC (wt.%)	Dielectric constant	Dielectric loss	A.C conductivity (S/cm)
0	2.86	0.46	2.54E-11
2	3.61	0.76	4.21E-11
4	4.19	0.88	4.89E-11
6	4.71	2.35	1.31E-10
8	5.37	3.38	1.88E-10

4.5 Application of (PMMA/Si_3N_4/TaC) Nanocomposites for Antibacterial Activity.

The (PMMA/Si_3N_4/TaC) nanocomposites were tested against gram-positive (Staphylococcus aureus) and gram-negative (Klebsiella aerogenes) and the results are shown in figures (4-21,4-22,4-23). From these figures, the inhibition zone for nanocomposites films was greater in gram-positive (Staphylococcus aureus) comparing than in gram-negative (Klebsiella aerogenes). The width of the inhibition zone rises with increasing Si_3N_4/TaC NPs concentration at (8 wt.%) and reaches its maximum value (25 mm) in case for gram-positive (Staphylococcus aureus). The reason for the bactericidal activity of nanostructures is due to the presence of (ROS) reactive oxygen species generated by nanoparticles. The electromagnetic interaction between the nanoparticles of nanocomposites and the bacteria will cause the germs to oxidize and die instantly since the nanocomposites contain positive charges while the microbes have negative charges. Singlet oxygen (O_2^-) may be the culprit for destroying the proteins and DNA of bacteria, and ROS, which includes radicals like super oxide radicals (O^{-2}), hydroxyl radicals (OH),

and hydrogen peroxide (H_2O_2), is the primary mechanism causing the antibacterial activity of nanocomposites by the nanoparticles [129,130].

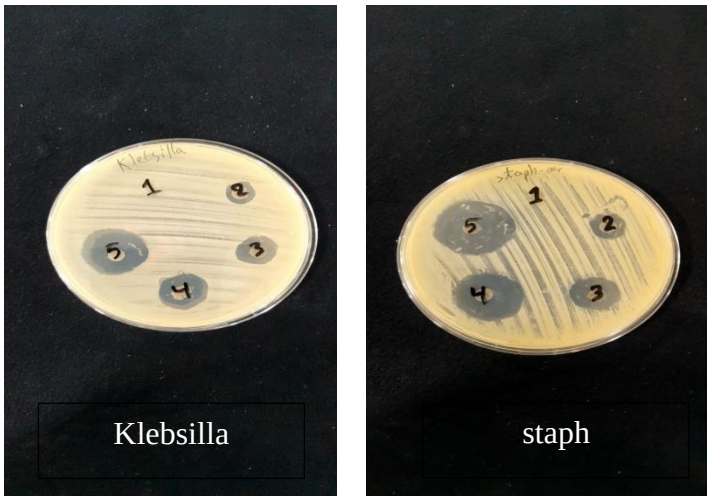

Fig. (4-21) Image for inhibition zonses of (PMMA/Si_3N_4/TaC) nanocomposite films on S. aureus and K. aerogenes.

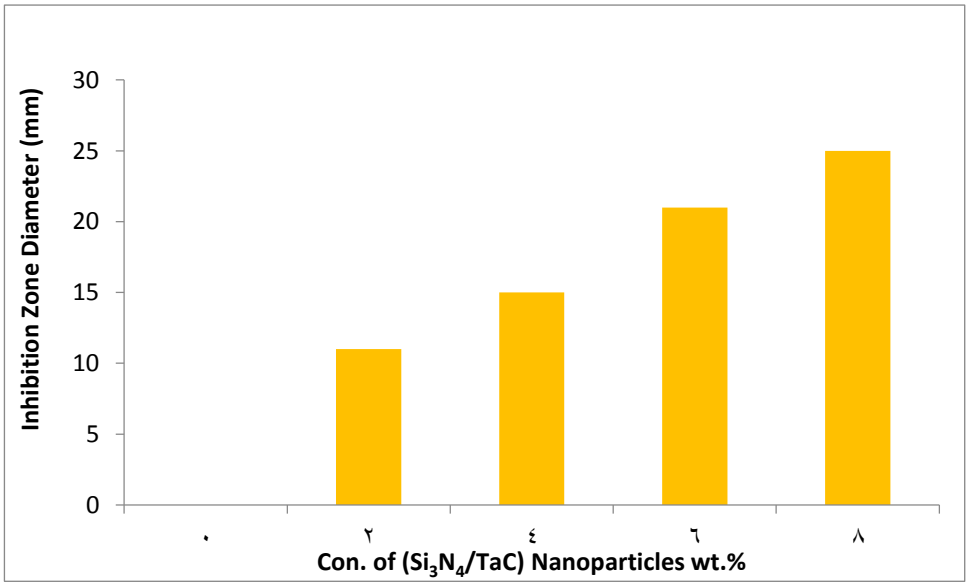

Fig. (4-22) Variation inhibition zone diameter of (PMMA/Si_3N_4/TaC) nanocomposite films on S. aureus with (Si_3N_4/TaC) concentration.

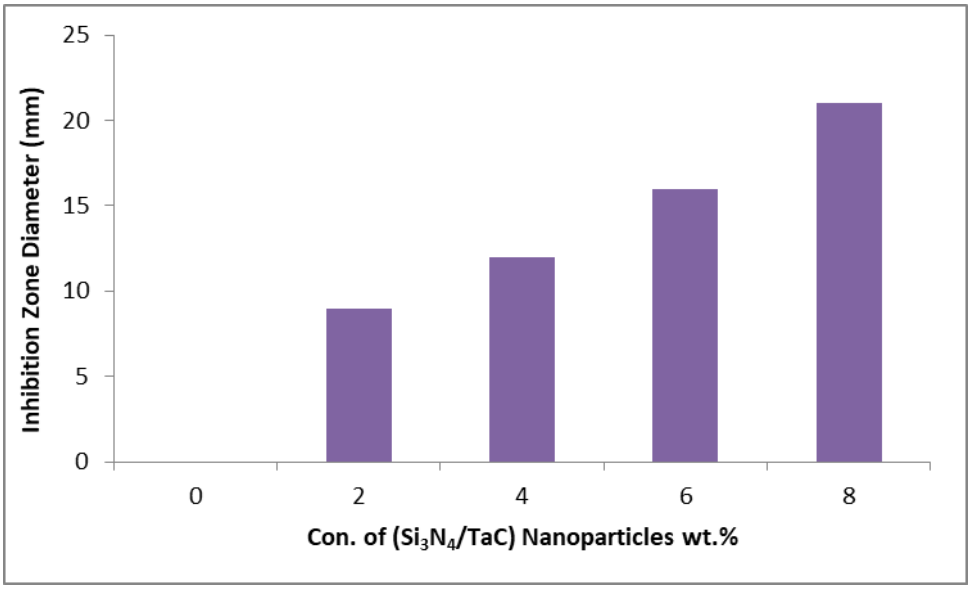

Fig. (4-23) Variation inhibition zone diameter of (PMMA/Si_3N_4/TaC) nanocomposite films on K. aerogenes with (Si_3N_4/TaC) concentration.

4.6 Conclusions

From the obtained results and discussions, the following points are concluded:

1- The optical microscope images show that Si_3N_4 and TaC nanoparticles form a continuous network inside the polymers when the ratio of (8) wt.%. FTIR spectra show a shift in some bands and change in the intensities of other bands comparing with pure PMMA film, this indicates there is no interaction between the polymers and the added nanoparticles. FE-SEM shows the surface morphology of the (PMMA/Si_3N_4/TaC) nanocomposites films with many aggregates or chunks randomly distributed on the top surface.

2- The absorbance, absorption coefficient, refractive index, extinction coefficient, dielectric constant (real, imaginary) and optical conductivity of (PMMA/Si_3N_4/TaC) nanocomposites increased with the increasing of the concentrations of the (Si_3N_4/TaC) nanoparticles. The transmittance and the energy gap for indirect transition (allowed, forbidden) decreased

with the increasing of the concentrations of (Si_3N_4/TaC) nanoparticles. This result can be used as anti-reflection coating.

3- The dielectric constant and dielectric loss for (PMMA/Si_3N_4/TaC) nanocomposites are increased with the increasing of (Si_3N_4/TaC) nanoparticles concentration and decreasing with the increase of frequency of the applied electric field. The A.C electrical conductivity increased with the increasing of nanoparticles concentration and frequency of the applied electric field. This result can be used as the electronic device.

4- The inhibition zone diameter increases with the increase in (Si_3N_4/TaC) nanoparticles concentrations.

4.7 Future works

1- Study the thermal and mechanical properties of (PMMA/Si_3N_4/TaC) nanocomposites.

2- Study the effect of radiation on some physical properties of (PMMA/Si_3N_4/TaC) nanocomposites.

3- Apply of (PMMA/Si_3N_4/TaC) nanocomposites as piezoelectric and photodetector.

References

References

[1] J. W. Nicholson, "Special topics in polymer chemistry" *J. Mater. Chem.*, Vol. 16, No. 39, pp. 3867–3874, (2006).

[2] J. M. G. Cowie and V. Arrighi, *Polymers: chemistry and physics of modern materials*. CRC press, (2007).

[3] N. Taniguchi "On the basic concept of nano-technology proceedings of the international conference on production engineering tokyo part ii japan society of precision engineering" *Pabbati al*, (1974).

[4] V. Sankar, T. S. Kumar, and K. P. Rao "Preparation, characterisation and fabrication of intraocular lens from photo initiated polymerised poly (methyl methacrylate)" *Trends Biomater. Artif. Organs*, Vol. 17, No. 2, pp. 24–31, (2004).

[5] M. Akay, *Introduction to polymer science and technology*. Bookboon, (2012).

[6] S. A. Salman, Z. A. Al-Ramadhan, and Z. F. Nazal, "Optical properties of polyvinyl alcohol (PVA) films doped with $CoCH_3COOH$ salt" *alcohol*, Vol. 2, p. 3, (2014).

[7] C. Yang, W. Li, Z. Yang, L. Gu, and Y. Yu "Nanoconfined antimony in sulfur and nitrogen co-doped three-dimensionally (3D) interconnected macroporous carbon for high-performance sodium-ion batteries" *Nano Energy*, Vol. 18, pp. 12–19, (2015).

[8] H. Al-Johani and M. A. Salam "Kinetics and thermodynamic study of aniline adsorption by multi-walled carbon nanotubes from aqueous solution" *J. Colloid Interface Sci.*, Vol. 360, No. 2, pp. 760–767,(2011).

[9] D. R. Paul and L. M.Robeson "Polymer nanotechnology: nanocomposites" *Polymer(Guildf)*, Vol.49,No.15,pp.3187–3204, (2008).

[10] S. Horikoshi and N. Serpone "Microwaves in Nanoparticle Synthesis, Published by Wiley" VCH Verlag GmbH & Co. KGaA, (2013).

[11] G. A. Kontos, A. L.Soulintzis, P. K. Karahaliou, G. C. Psarras, S. N Georga, C. A. Krontiras, and M. N. Pisanias "Electrical relaxation dynamics in TiO_2-polymer matrix composites" *Express Polym Lett*, Vol. 1, No. 12, pp. 781–789,(2007).

[12] S. Nagarajan and K. Arumugam Kuppusamy "Extracellular synthesis of zinc oxide nanoparticle using seaweeds of gulf of Mannar, India" *J. Nanobiotechnology*, Vol. 11, No. 1, pp. 1–11, (2013).

[13] S. Mustafa "Engineering Chemistry" Library of Arab society for pub. and dis, Jordan, (2008).

[14] A. C. Long and M. J. Clifford "Composite forming mechanisms and materials characterization" Composites forming technologies, pp.1-21, (2007).

[15] A. Muheisin "Study of electrical conductivity for amorphous and semi crystalline polymers filled with Lithium Fluoride Additive" M. Sc. Thesis, University of Mustansiriah, College of Science, (2009).

[16] J. M. Schultz "Polymer materials science", Prentice Hall, (1974).

[17] R. Klein "Laser Welding of Plastics" materials, processes and industrial applications, John Wiley and Sons, (2012).

[18] S. Amin and M. Amin "Thermoplastic Elastomeric (Tpe) Materials and Their Use in Outdoor Electrical Insulation" Rev. Adv. Mater. Sci.,Vol. 29, pp.15-30, (2011).

[19] J. Furer "Growth of Single-Wall Carbon Nanotubes by Chemical Vapor Deposition for Electrical Devices" Ph.D Thesis, Basel University (2006).

[20] K.T. Ramesh "Nanomaterials Mechanics and Mechanisms" The Johns Hopkins University, USA,P.3, (2009).

[21] D. Liu, W. Wu, Y. Qiu, S. Yang, S. Xiao, Q. Q. Wang, L. Ding, and J. Wang "Surface functionalization of ZnO nanotetrapods with photoactive and electro-active organic monolayers", J. of Langmuir, Vol.24, pp.5052-5059, (2008).

[22] C.Sun" Controlling the rheology of polymers/silica nanocomposites" thesis, Eindhoven University of Technology, (2010).

[23] M. Arifitekhar "Introduction to Composite Materials" Copyright © 2010, ASM International, (1999).

[24] J.J. Smit and P.H.F. Morshuis" Thermal and electrical properties of nanocomposites, including material processing" Ph.D. Thesis, Sai-Petersburg State Electrotechnical University 'LETI', Russia, (2012).

[25] A. Kurt "Influence of AlCl_3 on the optical properties of new synthesized 3-armed poly (methyl methacrylate) films" *Turkish J. Chem.*, Vol. 34, No. 1,pp. 67–80, (2010).

[26] H. Kaczmarek and H. Chaberska "The influence of UV-irradiation and support type on surface properties of poly (methyl methacrylate) thin films "*Appl. Surf. Sci.*, Vol. 252, No. 23, pp. 8185–8192, (2006).

[27] L. Nyangasi, D. Andala, C. Onindo, A. Wanyonyi, and J. Chepngetich "Processing parameters for electrospinning poly (methyl methacrylate)(PMMA)/titanium isopropoxide composite in a pump-free setup" *AAS Open Res.*, Vol. 1, p. 27, (2018).

[28] L. Premvardhan, L. A. Peteanu, P.-C. Wang, and A. G. MacDiarmid "Electronic properties of the conducting form of polyaniline from electroabsorption measurements" *Synth. Met.*, Vol. 116, No. 1–3, pp. 157–161, (2001).

[29] T. Webster, A. Patel, M. Rahaman, and B. Bal " Anti-infective and osteointegration properties of silicon nitride, poly(ether ether ketone), and titanium implants" Acta Biomater. Vol.8,pp. 4447–4454,(2012).

[30] H. Wu, L. Yang, J. Qian, D. Wang, Y. Pan, X. Wang, S. Nabanita, T. Tang, J. Zhao, and J. Wei " Microporous coatings of PEKK/SN composites integration with PEKK exhibiting antibacterial and osteogenic activity, and promotion of osseointegration for bone substitutes, ACS Biomater. Sci. Eng. Vol.5,pp. 1290–1301,(2019).

[31] R. Bock, B. McEntire, B. Bal, M. Rahaman, M. Boffelli, and G. Pezzotti "Surface modulation of silicon nitride ceramics for orthopaedic applications" Acta Biomater. Vol.26,pp. 318–330,(2015).

[32] Z. Xu, H. Wu, F. Wang, R. Kaewmanee, Y. Pan, D. Wang, P. Qu, Z. Wang, G. Hu, J. Zhao, R. Zhao, J. Wei " A hierarchical nanostructural coating of amorphous silicon nitride on polyetheretherketone with antibacterial activity and promoting responses of rBMSCs for orthopedic applications" J. Mater. Chem. B.Vol. 7,pp. 6035–6047,(2019).

[33] G. Pezzotti, R. Bock, B. McEntire, T. Adachi, E. Marin, F. Boschetto, W. Zhu, O. Mazda,and S. Bal "In vitro antibacterial activity of oxide and non-oxide bioceramics for arthroplastic devices: I. In situ time-lapse Raman spectroscopy" Analyst Vol.143,pp. 3708–3721,(2018).

[34] M. Ishikawa, K. Bentley, B. McEntire, B. Bal, E. Schwarz, and C. Xie" Surface topography of silicon nitride affects antimicrobial and osseointegrative propertiesof tibial implants in a murine model" J. Biomed. Mater. Res.Vol. 105,pp. 3413–3421,(2017).

[35] R. Bock, E. Jones, D. Ray, B. Bal, G. Pezzotti, and B. McEntire, "Bacteriostatic behavior of surface modulated silicon nitride in comparison to polyetheretherketone and titanium" J. Biomed. Mater. Res.Vol .105,pp. 1521–1534,(2017).

[36] B.J. McEntire, R. Lakshminarayanan, P. Thirugnanasambandam, J.S. Sampson, R. Bock, and D.O. Brien "Processing and Characterization of Silicon Nitride Bioceramics, Bioceram" Dev. Appl. Vol .6,pp. 1–9,(2016).

[37] M.H. Bocanegra-Bernal, and B. Matovic "Mechanical properties of silicon nitride-based ceramics and its use in structural applications at high temperatures" Mater. Sci. Eng. A. Vol.527,pp.1314–1338,(2010).

[38] E. Carrasquero, A. Bellosi, and M.H. Staia "Characterization and wear behavior of modified silicon nitride" Int. J. Refract. Met. Hard Mater. Vol . 23,pp. 391–397,(2005).

[39] A. E. Kaloyeros, Y.Pan, J. Goff & B. Arkles "Silicon nitride and silicon nitride-rich thin film technologies: state-of-the-art processing technologies, properties, and applications" *ECS Journal of Solid State Science and Technology*, Vol .*9*,No.6, p.63,(2020).

[40] Z.Krstic & V. D. Krstic " Silicon nitride: the engineering material of the future" *Journal of Materials Science*, Vol . *47,No.* 2,pp. 535-552,(2012).

[41] M.Vargas, HA.Castillo, E. Restrepo-Parra and W. De La Cruz "Stoichiometry behavior of TaN, TaCN and TaC thin films produced by magnetron sputtering" Appl. Surf. Sci. Vol .279,pp. 7–12,(2013).

[42] S .Du, M. Wen, Y. Qin, R. Li, H .Jin, P .Ren, W. Zheng, and X .Zhang Kand Bao "Optimizing the tribological behavior of tantalum carbide coating for the bearing in total hip joint replacement Vacuum . Vol .150, pp. 222–231, (2018).

[43] HM.Tütüncü, S.Bağci, S.Duman, E .Küçükerdoğan and GP.Srivastava "First-principles study of electronic and dynamical properties of the TaC(001) surface Diam" Relat. Mater. Vol .25,pp. 19–23,(2012).

[44] F. Peng, L .Han, X. FuH and Cheng "First-principles calculations on elasticity and the thermodynamic properties of TaC under pressure" Phys. Status Solidi Basic Res. Vol . 246,pp. 1590–6, (2009).

[45] M. Sahnoun, C. Daul, JC .Parlebas, M. Demangeat C and Driz "Electronic structure and optical properties of TaC from the first principles calculation" Eur. Phys. J. B .Vol . 44,pp. 281–6,(2005).

[46] Y.J. Chen, J.B. Li, and H.Z. Zhai "Preparation and growth mechanism of TaCx whiskers" J. Cryst. Growth. Vol . 224,pp. 244–250,(2001).

[47] O. Khyzhun, XPS, XES, and XAS "studies of the electronic structure of substoichiometric cubic TaCx and hexagonal Ta2Cy carbides" J. Alloys Compd. Vol .259,pp. 47–58,(1997).

[48] J.G. Choi "The influence of surface properties on catalityc activities of tantalum carbides" Appl. Catal. A. Vol .184,pp.189–201,(1999).

[49] A. Krajewski, L. D'Alessio, and G. De Maria "Physico-chemical and thermophysical properties of cubic binary carbides" Cryst. Res. Technol. Vol . 33,No. 3,pp. 341–374,(1998).

[50] M. Khusainov, G. Demyshav, and M. Myshlyaev "Mechanical properties and structure of carbide coatings of niobium and tantalum carbide" Russ. Metall. Vol .5 ,pp.144–146,(1990).

[51] D.J. Rowcliffe, and W.J. Warren "Structure and properties of tantalum carbide crystals" J. Mater. Sci. Vol . 5,pp. 345–350,(1970).

[52] O. C. Barraza "Process development and characterisation of (Ta, Hf) C ultra-high temperature ceramics" Doctoral dissertation, Imperial College London, (2015).

[53] Z. Zhang, H. Liang, H. Chen, J. Wang, F. Peng, & C. Lu " Exploring physical properties of tantalum carbide at high pressure and temperature" Inorganic Chemistry, Vol .59, No. 3, pp.1848-1852, (2019) .

[54] N. Sun, X. Meng, and Z. Xiao "Functionalized Si_3N_4 nanoparticles modified with hydrophobic polymer chains by surface-initiated atom transfer radical polymerization (ATRP)" *Ceramics International*, Vol. *41*, No.10, pp. 13830-13835, (2015).

[55] S. Natarajan, J. Kumari, D. S. Lakshmi, A. Mathur, M. Bhuvaneshwari, A. Parashar and A. Mukherjee "Differences in antibacterial activity of PMMA/TiO_2/Ag nanocomposite on individual dominant bacterial isolates from packaged drinking water, and their consortium under UVC and dark conditions" Applied Surface Science, Vol. 362, pp. 93-101, (2016).

[56] S. Singh, S. S. Dey, S. Singh & N. Kumar "Preparation and characterization of barium titanate composite film" *Materials Today: Proceedings, Vol .4*No.2,pp. 3300-3307, (2017).

[57] G. Soni, S. Srivastava, P. Soni, P. Kalotra, and Y. K. Vijay "Optical, mechanical and structural properties of PMMA/SiO2 nanocomposite thin films" *Mater. Res. Express*, Vol. 5, No. 1, p. 15302,(2018).

[58] D. Nayak and R. B. Choudhary "Augmented optical and electrical properties of PMMA-ZnS nanocomposites as emissive layer for OLED applications" *Opt. Mater. (Amst).*, Vol. 91, pp. 470 –481, (2019).

[59] G. Soni, N. Gouttam, and P. Soni "Optical properties of PMMA/ZnO/SiO_2 composite thin film" *Mater. Today Proc.*, Vol. 30, pp. 35–38,(2020).

[60] B. Yang, L. Sun, W.Wei, G. Niu, S. Chen, W. Wu& B. Li, "Fabrication and characterisation of geometry-controlled Cu microwires in porous poly (methyl methacrylate) templates using melt co-drawing and electrochemical deposition techniques" Materials & Design,Vol. 188, p.108453, (2020).

[61] X. Hu, S. Mei, F.Wang, S.Tang, D.Xie, C. Ding and J.A. Wei, "microporous surface containing Si_3N_4/Ta microparticles of PEKK exhibits both antibacterial and osteogenic activity for inducing cellular response and improving osseointegration" Bioactive Materials, Vol . 6, No.10,pp. 3136-3149, (2021).

[62] Q. A. Alsulami and A. Rajeh "Structural, thermal, optical characterizations of polyaniline/polymethyl methacrylate composite doped by titanium dioxide nanoparticles as an application in optoelectronic devices" *Optical Materials*, Vol. *123*, p.111820, (2022).

[63] D. B. Murphy, Fundamentals of light microscopy and electronic imaging. John Wiley & Sons,(2002).

[64] S.-N. Wang, F.-D. Zhang, A.-M. Huang, and Q. Zhou "Distinction of four Dalbergia species by FTIR, 2nd derivative IR, and 2D-IR spectroscopy of their ethanol-benzene extractives" Holzforschung, Vol. 70, No. 6, pp. 503–510, (2016).

[65] W. S. Lau, Infrared characterization for microelectronics. World scientific, (1999).

[66] S. Debbie "Principles and practice of variable pressure/ environmental scanning electron microscopy (VP-ESEM) "John Wiley & Sons, (2008).

[67] B. Pawley James "LVSEM for biology in Biological Low-Voltage Scanning Electron Microscopy "Springer, New York NY, pp.27-106, (2008).

[68] O. Stenzel, The physics of thin film optical spectra. Springer, (2015).

[69] A. M. I. F.H. Abdi El-kidder, N.A. Hakeem, I.S Ela Shumway "Structural, Optical and Thermal Characterization of ZnO Nanoparticles Doped in PEO/PVA Blend Films" Aust. J. Basic Appl. Sci., Vol. 7, No. 10, pp. 608–619, (2013).

[70] G. B. S. man C.M Wolfe, N. Hoouyak, Physical Properties of Semiconductors. Harlow, United Kingdom: Pearson Education Limited, (1989).

[71] Streetman, G.Ben and B. Sanjay "Solid state electronic devices " Prentice-Hall of India, (2001).

[72] A.G. Nilens "Deep imparity in Semiconductors" Wily-Inter Science Pubication, (1973).

[73] J.I. Pankove "Optical processes on semiconductors Dover publication" Inc. New york, (1971).

[74] M. Kittel,C. Charles and M.Paul "Introduction to solid state physics "New York: Wiley, Vol.8, (1996).

[75] P.Peinke, Joachim, Jürgen, E. R. Otto and S.Ruedi "Semiconductor physics" In Encounter with Chaos, Springer, Berlin, Heidelberg, pp.9-41, (1992).

[76] J. E. Jaffe and Z.Alex "Electronic structure of the ternary pnictide semiconductors ZnSiP 2, ZnGeP 2, ZnSnP 2, ZnSiAs 2, and MgSiP 2." Physical Review B, Vol. 30, No.2, p.741,(1984).

[77] Bonnell, B.Huey and D. Carroll "In-situ measurement of electric fields at individual grain boundaries in TiO_2." Solid State Ionics, Vol. 75, pp.35-42, (1995).

[78] J. Marien, T.Wagner, G. Duscher, A. Koch and M. Rühle "Nb on (110) TiO_2 (rutile): growth, structure, and chemical composition of the interface" Surface science, Vol.446, No.3, pp.219-228, (2000).

[79] M.N.Nnabuchi "Optical and solid state characterization of optimized manganese sulphide thin films and their possible applications in solar energy" The Pacific Journal of Science and Technology, Vol.7, No.1, pp.69-76, (2006).

[80] M. Davies, N. Hill, W. E. Vaughan, and A. H. Price "Dielectric properties and molecular behaviour" Hill,.., Vaughan, WE, Price, AH, Davies, M., Eds, (1969).

[81] K. Obeid "Preparation and Study Some of Electrical and Thermal Properties of a Nematic Liquid Crystal Material Prepared from Schiff Bases and Some its Complexes" M. Sc. Thesis, Babylon University, College of Science,(2010).

[82] L. Solymar and D. Walsh "Electrical Properties of Materials" 7th Edition Oxford University Press, Oxford, New York, (2004).

[83] D. J. Griffith, Introduction to Electrodynamics, 3rd Edition , Prentice Hall, Inc., New Jersey, USA, (1999).

[84] S. O. Gladkov, Dielectric Properties of Porous Media, Springer-Verlag Berlin Heidelberg, New York , USA, (2003).

[85] T. I. Zohdi, Electromagnetic Properties of Multiphase Dielectrics, A Primer on Modeling, Theory and Computation , Springer-Verlag Berlin, Heidelberg, Berkeley, USA, (2012) .

[86] W. Gao and N. M. Sammes, An Introduction to Electronic and Ionic Materials, World Scientific Publishing Co. Pte. Ltd., Singapore, (1999).

[87] M. M. Abutalib and A. Rajeh "Influence of ZnO/Ag nanoparticles doping on the structural, thermal, optical and electrical properties of PAM/PEO composite" *Phys. B Condens. Matter*, Vol. 578, p. 411796, (2020).

[88] K. M. E. Miedzinska, B. R. Hollebone, and J. G. Cook "An assigment of the optical absorption spectrum of mixed valence Co_3O_4 spinel films" *J. Phys. Chem. Solids*, Vol. 48, No. 7, pp. 649–656, (1987).

[89] B. Coşkun "Investigation of dielectric properties of Ag-doped ZnO thin films" *J. Mol. Struct.*, Vol. 1209, p. 127970, (2020).

[90] H. Jafar, N. Ali, and A. Shawky "Study of A . C Electrical Properties of Aluminum – Epoxy Composites" Al-Nahrain Journal of Science, Vol. 14, No. 3, pp. 77–82, (2011).

[91] T. Seghier and F. Benabed "Dielectric Proprieties Determination of High Density Polyethylene (HDPE) by Dielectric Spectroscopy" Int. J. Mater. Mech. Manuf., vol. 3, No. 2, pp. 121–124, (2015).

[92] S. Shekhar, V. Prasad, and S. Subramanyam "Structural and electrical properties of composites of polymer-iron carbide nanoparticles embedded in carbon" Mater. Sci. Eng. B Solid-State Mater. Adv. Technol., Vol. 133, No. 1–3, pp. 108–112, (2006).

[93] T. Furukawa "Electrical properties of polymers" Reports Prog. Polym. Phys. Japan, Vol. 43, pp. 369–390,(2000).

[94] R. Dorf, The Electrical Engineering Hand Book, CRC Press LLC, 2nd Edition, Piscataway, New Jersey, USA, pp.1-2976 (2000).

[95] R. AL-Morshdy, M. Habeeb, and H. AL-Asadi "Effect of Nanosilver Particles on the Optical and Structural Properties of (PVA-PVP) Films" Advances in Physics Theories and Applications, Vol. 34, No. January,PP.30-39, (2014).

[96] N. Azahari, N. Othman, and H. Ismail "Biodegradation studies of polyvinyl alcohol/corn starch blend films in solid and solution media" J. Phys. Sci., Vol. 22, No. 2, pp 15–31,(2011).

[97] I. Yücedaug, A. Kaya, C.Semsettin Altindal, and I. Uslu "Frequency and voltage-dependent electrical and dielectric properties of Al/Co-doped {PVA}/p-Si structures at room temperature" Chinese Phys. B, Vol. 23, No. 4, P. 47304, Apr. (2014).

[98] H. Li, Q. Chen, J. Zhao, and K. Urmila "Enhancing the antimicrobial activity of natural extraction using the synthetic ultrasmall metal nanoparticles" Sci. Rep., Vol. 5, No. 1, pp. 1–13, (2015).

[99] I. Armentano, C. R. Arciola, E. Fortunati, D. Ferrari, S. Mattioli, C. F. Amoroso, J. Rizzo, J. M. Kenny, M. Imbriani, and L. Visai "The interaction of bacteria with engineered nanostructured polymeric materials: a review" Sci. World J., Vol. 2014, (2014).

[100] L. G. Harris, S. J. Foster, and R. G. Richards "An introduction to Staphylococcus aureus, and techniques for identifying and quantifying S. aureus adhesins in relation to adhesion to biomaterials: review" *Eur Cell Mater*, vol. 4, no. 3, pp. 100–120, 2002.

[101] V. P. Kumar, N. S. Chauhan, H. Padh, and M. Rajani "Search for antibacterial and antifungal agents from selected Indian medicinal plants" *J. Ethnopharmacol.*, vol. 107, no. 2, pp. 182–188, 2006.

[102] E. A. Roe, R. J. Jones, R. E. Dyster, "Passive immunization of mice against Klebsiella aerogenes" British journal of experimental pathology, Vol. 67, No.1, p.25, (1986).

[103] M. Rezvanpour, M. Hasanzadeh, D. Azizi, A. Rezvanpour and M. Alizadeh “Synthesis and characterization of micro-nanoencapsulated n-eicosane with PMMA shell as novel phase change materials for thermal energy storage” Mater. Chem. Phys., Vol. 215, pp. 299–304, (2018).

[104] J. B. Ramesh and K. K. Vijaya “Studies on structural and electrical properties of NaHCO3 doped PVA films for electrochemical cell applications” Chemtech, Vol.7, pp. 171–180, (2014).

[105] A. Paydayesh, , A. A. Azar & A. J. Arani, "Investigation the effect of Graphene on The Morphology, Mechanical and Thermal properties of PLA/PMMA Blends" Ciência e Natura, Vol . 37, PP.15-22,(2015)

[106] L. Chaudhari and R. Nathuram " Absorption Coefficient of Polymers (Polyvinyl Alcohol) by Using Gamma Energy of 0.39MeV" Bulg. Journal of Physics,Vol.37,PP.232–240,(2010).

[107] S. Kolpakov, N. Gordon, C. Mou, and K. Zhou " Toward a New Generation of Photonic Humidity Sensors" Journal of Sensors, Vol.14, PP. 3986-4013; doi:10.3390/s140303986,(2014).

[108] N. D. Md Sin, M. F. Tahar, M. H. Mamat and M. Rusop " Enhancement of Nanocomposite for Humidity Sensor Application" Journal of Recent Trends in Nanotechnology and Materials Science, Engineering Materials, DOI: 10.1007/978-3-319- 04516-0_2, P. 15-31, PP. 15-30,(2014).

[109] N. B. Rithin Kumar, V. Crasta, R. F. Bhajantri and B.M. Praveen "Microstructural and Mechanical Studies of PVA Doped with ZnO and WO_3 Composites Films" Journal of Polymers, Vol. 2014, Article ID 846140,P. 7,(2014).

[110] J. R. Babu and K.V. Kumar "Studies on Structural and Electrical Properties of $NaHCO_3$ Doped PVA Films for Electrochemical Cell Applications" International Journal of Chem. Tech. Research, Vol.7, No. 1, PP.171-180, (2014).

[111] S. H. Borova, O. M. Shevchuk, N. M. Bukartyk, E. Y. Nikitishyn and V. Tokarev "Nanocomposite Films Based on Functional Copolymers with Embedded Carbon Nanotubes" proceedings of the International Conference Nanomaterials: Applications and Properties, Vol. 3, No. 2,(2014).

[112] S. Salman, N. Bakr and M. H. Mahmood "Preparation and study of some optical properties of (PVA- $Ni(CH_3COO)_2$) composites" International Journal of Current Research, Vol. 6, Issue, 11, PP.9638-9643,(2014).

[113] S. A. Mahmoud, A. A. Akl, H. Kamal, and K. Abdel-Hady "Opto-structural, electrical and electrochromic properties of crystalline nickel oxide thin films prepared by spray pyrolysis" *Phys. B Condens. Matter*, vol. 311, no. 3–4, pp. 366–375, 2002.

[114] K. Karthikeyan, N. Poornaprakash, N. Selvakumar and Jeyasubrmanian "Thermal Properties and Morphology of MgO-PVA Nanocomposite Film" Journal of Nanostructured Polymers and Nanocomposites, Vol. 5, No. 4, PP. 83-88,(2009).

[115] N. Elmarzugi1, T. Adali, A. Bentaleb, E. I. Keleb, A. T. Mohamed and A. M. Hamza" Spectroscopic Characterization of PEG- DNA Biocomplexes by FTIR" Journal of Applied Pharmaceutical Science, Vol. 4, No. 8, PP. 6-10, (2014).

[116] N. Arsalani, H. Fattahi and M. Nazarpoor " Synthesis and characterization of PVP-functionalized super paramagnetic Fe_3O_4

nanoparticles as an MRI contrast agent" Journal of express Polymer Letters Vol.4, No.6, PP. 329–338,(2010).

[117] D. Kumar, S. Karan Jat, P. K. Khanna, N. Vijayan, S. Banerjee "Synthesis, Characterization, and Studies of PVA/Co-Doped ZnO Nanocomposite Films" International Journal of Green Nanotechnology, Vol. 4, PP.408–416, (2012).

[118] C. Srikanth, C. Sridhar, B. M. Nagabhushana and R.D.Mathad " Characterization and DC Conductivity of Novel CuO doped Polyvinyl Alcohol (PVA) Nano-composite Films " Journal of Engineering Research and Applications, Vol. 4, Issue 10, PP.38-46,(2014).

[119] S. D. Meshram, R. Rupnarayan, S. V. Jagtap, V. G. Mete and V. S. Sangawar " Synthesis and Characterization of Lead Oxide Nanoparticles" International Journal of Chemical and Physical Sciences, Vol. 4, Special Issue, PP. 83-88,(2015).

[120] G. H. Murhekar and A. R. Raut " Electrical properties of modified polyvinyl alcohol conjugates and doped modified polyvinyl alcohol conjugates" International Journal of Chemical Studies, Vol. 2, Issue 2, PP. 77-82,(2014).

[121] S. Ahmad and S. A. Agnihotry "Synthesis and characterization of in situ prepared poly (methyl methacrylate) nanocomposites" Bull. Mater. Sci., Vol. 30, No.1, pp. 31–35, (2007).

[122] S. Ramesh and L. C. Wen "Investigation on the effects of addition of SiO_2 nanoparticles on ionic conductivity, FTIR, and thermal properties of nanocomposite PMMA–$LiCF_3SO_3$–SiO_2" Ionics (Kiel)., Vol. 16, No. 3, pp. 255–262, (2010).

[123] Y. Haghighi, Mojtaba and L. Pearl "FTIR analysis of a polycarbonate blend after hygrothermal aging" Journal of Applied Polymer Science, Vol.132, No.3, (2015).

[124] A. Goswami, A. K. Bajpai and B. K. Sinha “Designing vanadium pentoxide-carboxymethyl cellulose/polyvinyl alcohol-based bionanocomposite films and study of their structure, topography, mechanical, electrical and optical behavior” Polym. Bull., Vol.75, No.2, pp.781–807, (2018).

[125] K. Rajesh, V. Crasta, K. N. B. Rithin, G. Shetty and P. D. Rekha “Structural, optical, mechanical and dielectric properties of titanium dioxide doped PVA/PVP nanocomposite” J. Polym. Res., Vol.26, No.4, pp.1-10, (2019).

[126] G. Chakraborty, K. Gupta, D. Rana and A. M. Kumar "Dielectric relaxation in polyvinyl alcohol–polypyrrole–multiwall carbon nanotube composites below room temperature" Advances in Natural Sciences, Vol. 4, pp. 1-4, (2014).

[127] S. .Ju1, M. Chen, H. Zhang and Z. Zhang “Dielectric properties of nanosilica/low-density polyethylene composites: The surface chemistry of nanoparticles and deep traps induced nanoparticles" Journal of express Polymer Letters, Vol.8, No.9, pp.682–691, (2014).

[128] O. Abdullah, G. M. Jamal, D. A. Tahir. And S. R. Saeed "Electrical Characterization of Polyester Reinforced by Carbon Black Particles" International Journal of Applied Physics and Mathematics, Vol. 1, No.2, pp.101-105, (2011).

[129] Y. T. Prabhu, K. V. Rao, B. S. Kumari, V. S. S. Kumar, and T. Pavani "Synthesis of Fe_3O_4 nanoparticles and its antibacterial application" Int. Nano Lett., Vol. 5, No. 2, pp. 85–92, (2015).

[130] G. Asab, E. A. Zereffa and A. T. Seghne, "Synthesis of silica-coated Fe_3O_4 nanoparticles by microemulsion method: Characterization and evaluation of antimicrobial activity" International journal of biomaterials, Vol. 2020, (2020).

الخلاصة

في هذه الدراسة، حضر المتراكب النانوي (PMMA/Si_3N_4/TaC) باستخدام طريقة الصب بنسب وزنية مختلفة من جسيمات Si_3N_4/TaC النانوية (2 ,4 ,6 و 8). wt% . شخصت الخصائص التركيبية والسطحية والبصرية والكهربائية للمتراكب النانوي (PMMA/Si_3N_4/TaC). أظهرت صور المجهر الضوئي توزيع الجسيمات النانوية Si_3N_4/TaC بشكل شبكة مستمرة داخل البوليمر عند النسبة (8 wt.%). اظهر طيف (FTIR) زحف في بعض القمم وزيادة في شدة لقمم اخرى مقارنة مع الغشاء (PMMA) وهذا يشير بانه لا يوجد تفاعل بين البوليمر والمواد النانوية المضافة. اظهرت صور (FE-SEM) لسطح الأغشية للمتراكب النانوي (PMMA/Si_3N_4/TaC) توزيع متجانس ومنتظم للجسيمات النانوية داخل المصفوفة البوليمرية. أظهرت نتائج الخصائص البصرية للمتراكب النانوي بأن الامتصاصية، معامل الامتصاص، معامل الانكسار، معامل الخمود، ثابت العزل الحقيقي والخيالي، التوصيلية البصرية تزداد مع زيادة تركيز جسيمات النانوية Si_3N_4/TaC. النفاذية وفجوة الطاقة للانتقال غير مباشر (المسموح والممنوع) تقل مع زيادة تركيز جسيمات النانوية Si_3N_4/TaC. اظهرت نتائج الخصائص الكهربائية المتناوبة (A.C) تزداد مع زيادة تركيز جسيمات النانوية Si_3N_4/TaC وتتناقص مع زيادة تردد المجال الكهربائي المسلط. التوصيلية الكهربائية المتناوبة (AC) تزداد مع زيادة تركيز جسيمات النانوية Si_3N_4/TaC والتردد. اختبرت المتراكبات النانوية (PMMA/Si_3N_4/TaC) كمضادات لبكتريا موجبة غرام (المكورات العنقودية الذهبية) وسالبة غرام (الكليبسيلا المعوية) وبينت النتائج أن منطقة التثبيط ازدادت بزيادة تراكيز الجسيمات النانوية Si_3N_4/TaC.

جمهورية العراق
وزارة التعليم العالي والبحث العلمي
جامعة بابل
كلية التربية للعلوم الصرفة
قسم الفيزياء

تأثير الجسيمات النانوية Si_3N_4/TaC على خصائص PMMA كمضاد بكتيري

رسالة مقدمة

الى مجلس كلية التربية للعلوم الصرفة في جامعة بابل وهي جزء من متطلبات درجة الماجستير في التربية/ الفيزياء

من قبل الطالبة

الاء عباس محمد طلفاح

بكالوريوس تربية فيزياء

جامعة بابل/٢٠٠٩

بأشراف

أ. د. مجيد علي حبيب

١٤٤٤ هـ

٢٠٢٣ م